The effects of moisture conditioning on the mechanical properties of the fused deposition modeling printed carbon fiber reinforced composites

Name: **Zitong Zhang**

SID: 430415441

Supervisor:

Dr. **Li Chang**

(Prof. Lin Ye)

A thesis submitted in fulfilment of the requirements for the degree of

Master of Philosophy

School of Aerospace, Mechanical & Mechatronic Engineering

Faculty of Engineering

The University of Sydney

Declaration

I declare the concept and work in this thesis has not been previously submitted for other degree. The thesis is written by myself. I designed the experiment, prepared the samples and carried out all the experiments on my own. Assistances I have received in my research and preparation of the thesis are acknowledged. All the sources of information and relevant literatures are well referenced.

As a supervisor for the candidature on which this thesis is based, I can confirm that the authorship declaration statements mentioned above are correct.

Supervisor: Dr Li Chang

Date 28/12/2022

Acknowledgement

I would like to give my sincere appreciation to my supervisor Dr. Li Chang for his long lasting support throughout my research work, for his conceptualization, guidance and suggestions.

I am very grateful for the support provided by Dr Andy Wang for helping my experiments, answering my concerns and provide advice on my thesis. I would also thank Zhiwang Li for helping me the work regarding SEM. Without their help, there is no way for me to finish the thesis on time.

List of Tables

List of Figures

Table of content

Abstract

The aims of this thesis is to evaluate the effects of moisture conditioning on the mechanical and tribological properties of the fused deposition modeling (FDM) printed carbon fiber reinforced composites.

It was found that printed materials show faster and higher absorption rates, compared to the polymeric materials prepared using traditional processing methods reported in literature. With the presence of fiber reinforcements e.g., ~ 10vol.% short carbon fibers, the absorption rate can be further increased, due to the formation voids. However, with a relative high volume fracture of continuous carbon fiber (~35vol.%), the water absorption may decrease.

Tensile tests were conducted on both short fibers and continuous fiber reinforced polymers, to investigate the effects of the defects in FDM printed polymer composites on their moisture absorption behavior and mechanical properties. The moisture absorption resulted in more noticeable damage on the tensile strength of polymer composites filled with short fiber than those with continuous fibers. This can be explained by the fact that the tensile properties of the short fiber reinforced composites are greatly dependent on the bonding strength between fiber-polymer, which can be significantly deteriorated due to the moisture absorption. On the other hand, with continuous fiber reinforcements, the mechanical properties of polymer composites were more dependent on fibers, which is less sensitive to the moisture absorbed in polymer matrix.

The friction and wear behavior under moisturized conditions of short and continuous fiber reinforced polymer was investigated. The tribological performance of the short carbon fiber reinforced polymer tends to decrease when the moisture level increased in material. However, for continuous carbon fiber reinforced polymer, the friction and wear may decrease with the water absorption, especially an under low relatively load.

Based on scanning electron microscope observations, the underlying wear mechanisms were further discussed.

Scratch tests were conducted to study the surface damage mechanism of additively manufactured short carbon fiber (SCFC) and continuous carbon fiber composites (CCFC). The fiber-nylon debonding was particularly investigated. Different scratch modes were identified under different normal loads; namely abrasion, nylon debris formation, nylon ripple like formation, fiber breakage, fiber removal and surface collapsing. In particular, the main damage mechanism in short fiber reinforced composites was the plastic deformation of nylon matrix; whilst in the continuous fiber reinforced composites, the main damage mechanism is the crack formation in fiber-nylon interfacial region. With the increase of normal load, fiber could be damaged and removed from the surface of SCFC. In CCFC, crack formed on nylon matrix surface with more fiber breakage.

Finally, to further explore the failure behavior of fiber under a moisturized condition, a finite element model was also established to analyze the stress distribution in the contact region. The results showed that the stress distribution in composite specimens is dependent on a number of factors such as volume fraction of fiber, scratch indenter size and softening effect of nylon under the moisturized condition. The stress distribution contour revealed a strong correlation between the tribology and scratch experiment carried out in this thesis. It contributed to a deeper understanding of scratch and tribology performance of 3D printed fiber reinforced polymers. The work provided a theoretic foundation for the design and development of high wear resistant fiber-reinforced polymer composites using 3D printing technology for various tribology applications.

Chapter 1. Introduction

1.1 An introduction of application and characteristics of polymers

Nowadays, polymers are widely used in multiple sectors, including aerospace, medical, automotive industries. Polymers have a great demand because of their excellent performance to weight ratio. Compared with metals, polymers have many advantages. They are more resistant to chemicals. With a similar mechanical performance, polymers and composite materials can be ten times lighter than metals. In addition, polymer structure is easy to be cleaned and sterilized. All these advantages make polymers ideal candidates for many applications. However, polymers also have drawbacks. For example, polymers are weakened and melted at high temperature. The disposal issue remains unsolved and recycling progress is still under investigation. Also, mechanical properties of polymer can be changed significantly under a water or humidify condition, giving challenges for many applications.

Research has shown that [1, 2] the increase of moisture level decreased polymer-composites' the tensile strength, tensile modulus and flexural modulus significantly. Meanwhile, under the same moisture gain, polymers exposed to humidify environment or immerse in water at a higher temperature decreased the mechanical property further.

1.2 The history of additive manufacturing

Additive manufacturing (AM), namely 3D printing, is a manufacturing process that fabricates objects from three dimensional models. In last few decades, numerous AM processes have been developed in many industries [3]. Unlike the conventional manufacturing process, additive manufacturing builds the objects layer by layer. This offers flexibility, freedom of design, and low cost production.

The mainstream AM production methods include stereolithography (SL), laminated object manufacturing (LOM), fused deposition modeling (FDM) and selective laser

sintering (SLS) [4]. FDM technology accounts for the largest market share because of the matured technology. The parts of FDM involve filament, liquefier, print head, gantry and build surface [5]. It follows the printing progress that extruding a material from filament type and then depositing on a platform. It creates a 2D layer on top of another. At last, all layers stack altogether to form a three dimensional object [6].

FDM technique is based on material-melting in which a spool of thermoplastic filament is melted and extruded through a heated nozzle. The melted filament instantly solidifies when it is laid on the platform. Once the whole layer has completed the laydown process, the printing bed moves down controlled by the 3D printer motor and the next layer is prepared to lay down.

Despite the easy manufacturing process, FDM printed parts have disadvantages. FDM printed technique creates voids, micro porosities and imperfect gaps in the printed parts. These defects significantly decrease the mechanical performance of the printed samples. To tackle them, many techniques have been implemented to strengthen the FDM printing. One way is to add reinforced fiber. Wang et al [7] stated that adding short-fiber reinforcements into FDM parts could significantly increase the mechanical performance. Another approach of strengthening is to print continuous fiber reinforced polymers. Continuous fiber reinforcements include continuous carbon fiber, fiberglass and Kevlar fibers [8]. These aligned fibers can effectively improve the mechanical performance of polymer matrices, giving their great potentials for many engineering applications [9, 10].

Polymers are hygroscopic, i.e., they are moisture sensitive. This behavior must be considered during material design, mechanical performance prediction and optimization. The moisture content in polymer is a key variable affecting processing and end-use performance. It affects material properties including strength, stiffness, and ductility [1, 26].

1.3 Research aims

To date, publications have concluded that the moisture gives a negative effect on the mechanical performance of polymer manufactured by conventional manufacturing method. However, few literatures have focused on investigating the moisture effect on 3D printed composites' deformation behavior. In particular, the differences of micro structure between conventional manufacturing progress and FDM printed composites have not been well investigated. Thus, the thesis aims to investigate the moisture effect of mechanical properties on FDM printed objects.

In the thesis, the work organizations are shown as follow:

1. FDM printed neat polymer, short fiber and continuous fiber composites were selected and fabricated.
2. Tensile tests in neat and fiber polymer composites in moisturized condition were carried out and compared with the results of those of injection molded polymer.
3. Tribology and scratch tests of short fiber and continuous fiber were carried out to observe and analyze the damage mechanism under a dry and water absorbed conditions. Extra attention was paid to observe the damage pattern on fiber and fiber-polymer interfacial bonding.
4. A finite element model (FEM) of scratching over a fiber-polymer composite surface was developed to analyze the stress distribution in the contact region. Emphasis was made on what other scratch factors could affect the scratch stress distribution. The model was also applied to interpret the tribological performance of the printed composite materials.

The thesis includes the following main chapters;

Scratch damage mechanism on fiber-polymer composites surface is reviewed. Chapter 3 illustrates the experiment preparation of 3D printed fiber composites and procedure of moisturized conditioning. The numerical modeling is discussed. Chapter 4 compares the effects of moisture conditioning methods of tensile properties of 3D printed fiber-polymer composites. Chapter 5 shows the tribology experimental results of fiber-polymer composite under a moisturized condition. Chapter 6 presents the experimental and numerical investigation of scratch performance of fiber composites under different scratching conditions.

Chapter 2. Literature Review

2.1 Mechanical characteristics of additive manufacturing by Fused Deposition Modeling (FDM)

2.1.1 Mechanical properties of composites with short carbon fiber reinforced Composites (SCFC)

Short fiber introduced in polypropylene (PP) results in a massive improvement for modulus and strength [11, 12]. Yield strength, ultimate strength and ductility of short carbon fiber reinforced composites have been investigated [13, 14]. The printed objects had the following characteristics: Tensile properties were maximized when filament and fiber were longitudinally aligned to the loading direction, while mechanical performance was poorest when fiber was perpendicular to the loading direction [15]. Pre-fabricated fiber-polymer filament contained voids, which results in stress concentration and failure unexpectedly [24]. The void generally deteriorated the mechanical properties of FDM.

2.1.2 Mechanical properties of printed composites with continuous carbon fiber reinforced Composites (CCFC)

Continuous carbon fiber reinforced composites show that they offer a significant improvement of mechanical properties [4]. Matsuzaki et al [16] studied in-nozzle impregnation of continuous fiber and thermoplastic resin. They compared the results of mechanical properties with short carbon fiber polylactic acid. The ultimate tensile strength and young's modulus of CCFC were 300% higher than SCFC [16]. Namiki et al [17] printed polylactic acid with continuous fiber, showing a similar result. This was confirmed by Yu. T et al [18]. Air gaps and weak bonding between PLA matrix and continuous carbon fiber might impact on the mechanical properties. Compared with SCFC, there were more gaps and porosities in CCFC.

By using Mark Forged Company's printing platform, Miguel et al [19] studied the compressive and flexural properties of continuous fiber fabrication in order to investigate the effect of fabrication parameters. A 1:1 of nylon 6 (PA6): carbon fiber layer ratio for 24.44% of carbon fiber volume achieved a maximum compressive modulus of 2.1GPa which was 126%-140% higher than traditional FDM 3D printed Acrylonitrile butadiene styrene plastic [20, 21]. Maximum flexural Modulus was achieved in a carbon fiber volume fraction of 48.93% with a value of 14.17GPa. This was 29 times higher than that of the 3D printed Acrylonitrile butadiene styrene plastic objects reported by Z. Weng et al [22]. Fiber delamination and debonding were observed in figure 1. This indicated a poor adherence between fiber and polymer. The formation of porosities was reported by J Justo et al [23]. The study showed that the formation of many porosities was due to the absence of pressure of manufacturing the thermoplastic-based composites.

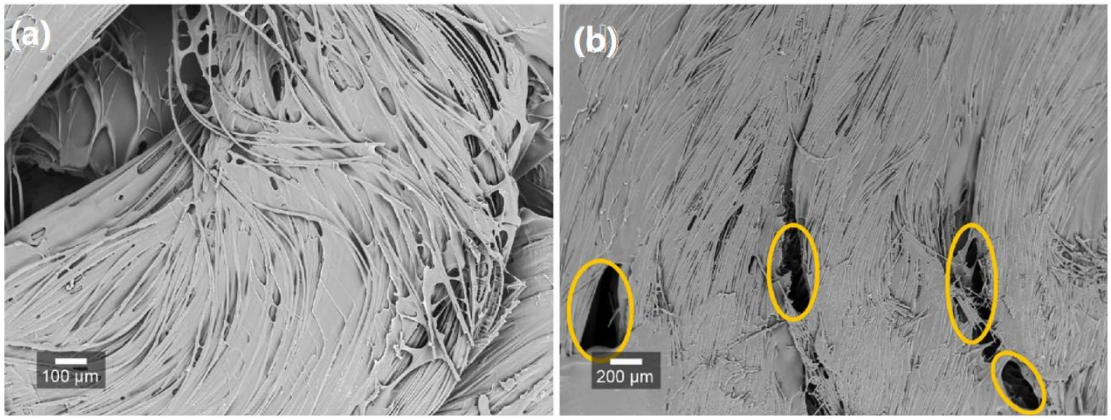

Figure 1. CCFC specimens and the present of voids between printed fiber filament [20].

To further investigate the effect of microscopic voids on mechanical performance of 3D printed CCFC composites, Qinghao et al [24] used the micro-CT to determine the fiber and void volume fraction. It was found that the carbon fiber volume was $34 \pm$

0.8%, and the void volume was from 10.3% to 14.3%, respectively. The void volume fraction was much higher than composite laminates manufactured by traditional techniques, presenting in figure 2. Qinghao et al calculated the theoretical tensile strength by using the rule of mixture equation, concluding that the experimental results showed a much lower value than theoretical calculation. This indicated the negative effect of voids. The authors further used the compression moulding (CM) process to eliminate voids in the specimens. Compared with the untreated specimens, there was a huge improvement of composites' tensile and flexural strength after CM treatment. Longitudinal tensile strength and modulus increased 22.5% and 36.4%, while transverse tensile strength and modulus increased 78% and 100%, respectively. Longitudinal flexural strength and modulus increased 93% and 60%, respectively. Therefore, it was concluded that the existence of voids posted a great effect on longitudinal flexural and transverse tensile specimens. Continuous carbon fiber with poor support of surrounding nylon matrix caused the premature failure. The use of CM highlighted the negative effectiveness of voids on 3D printed objects mechanical performance.

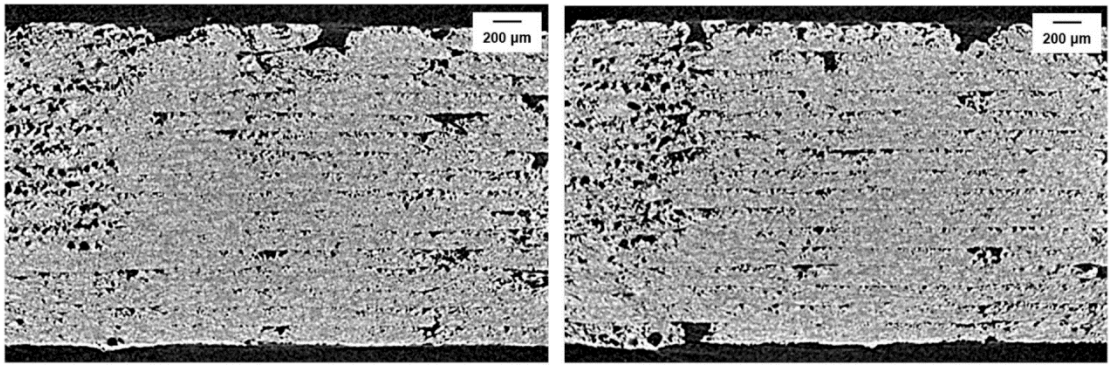

Figure 2. A cross-section micro-CT view of the CCFC sample [24]

The bonding performance of the interface between continuous fibers and polymer matrix was investigated by M.A Caminero et al [25]. Inter-laminar failure initially

occurred between the fiber and polymer. Increasing fiber content led to more air inclusions in the composites, especially in the areas where were close to fiber bundles and polymer matrix. Figure 3 shows the porosities and fiber pullout, indicating a poor interface bonding. This eventually weakened the mechanical performance of printed objects.

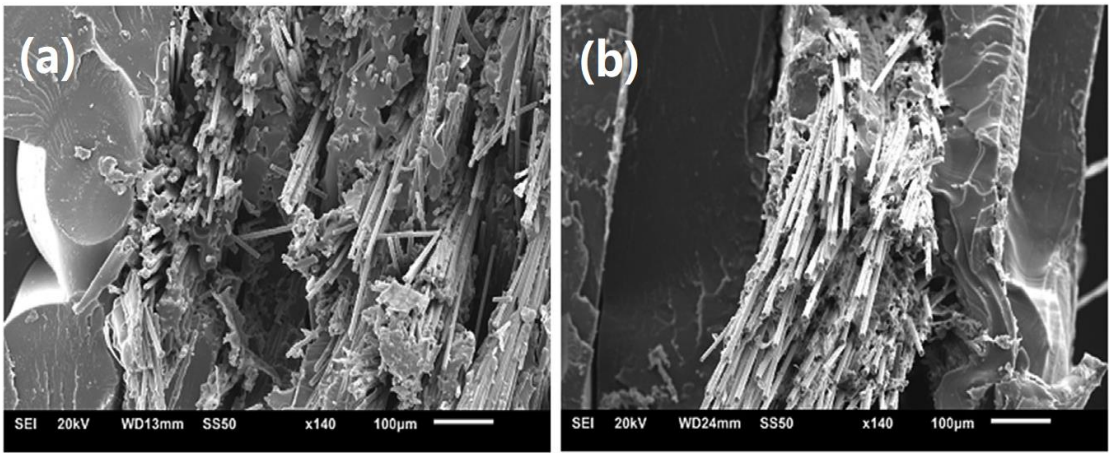

Figure 3. SEM of interface of fiber-nylon polymer on fracture surfaces [25].

2.2 Polymer in moisturized conditions.

2.2.1 The changes of molecular structure of polymer in moisturized condition

Song and Ehrenstein et al [26] found that the uptake was caused by the polar amide groups having an affinity for water. Water molecules loosen the existing hydrogen bonds and formed its own hydrogen bonds with the amide group, presenting in figure 4. The change of molecular structure of nylon gives PA6 to close to a viscoelastic behavior [27].

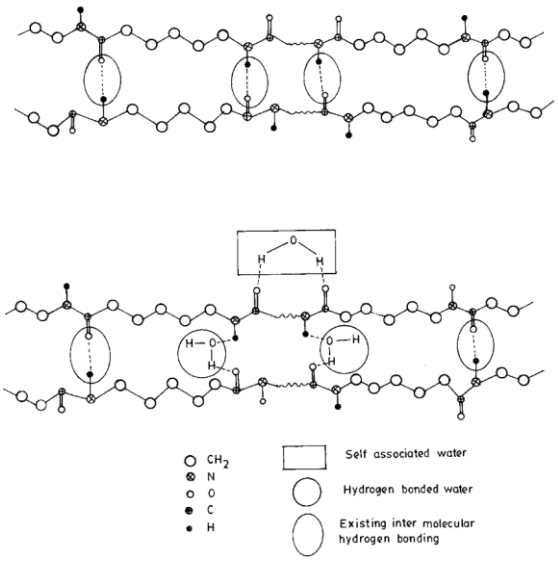

Figure 4. The change of molecule structure of polymer (PA6) when moisturized.

2.2.2 Effects of moisture conditioning on mechanical properties of nylon polymer PA6.

Nan et al [1] investigated the moisture condition methods on mechanical performance of nylon 6. They immersed neat nylon 6 in water from 0 to 2000hours with different temperatures, and evaluated the mechanical properties of nylon under moisturized conditions. Tensile stress, tensile modulus, flexural stress and flexural modulus associated with moisture levels were examined. They reported nylon 6 was able to absorb up to 10wt% of moisture in a time length of 2000hours. The equilibrium moisture was greatly dependent on temperature. Meanwhile, the mechanical properties of nylon 6 were greatly influenced by moisture levels. Tensile and flexural stress reduced 70% if moisture level reached 10wt%, while tensile and flexural modulus decreased 5 times.

2.2.3 Effects of moisture conditioning of carbon fiber reinforced composites manufactured by traditional techniques.

A.G. Airale et al studied the moisture effect on mechanical properties of polymeric composite materials [29]. They selected Epoxy Resin (EP) with E-glass or carbon fiber (T300), PolyPhenylene Sulfide (PPS) with E-glass or (T300) for advanced composites, all manufactured out of prepare plies and cured in an autoclave. Samples were moisturized according to standard ASTM D5229 [30]. The results indicated that up to 0.8% moisture was absorbed by traditional curing method. There was a 5% decrease of young's modulus for E-glass/EP. Tensile strength slightly dropped for around 8-10%, while the strain decreased 12%. The experiment concluded that comparing with neat nylon, moisture effect on polymeric composite materials was less obvious.

2.3 Tribology performance of carbon fiber reinforced composites

Tribology performance is one of the most important indicators for examining the mechanical properties of materials. Polymer composites are widely used as sliding elements in a range of industrial applications. It is well known that adding short fiber into the neat polymers could dramatically improve the load carrying capacity, due to a reduction of plowing, tearing and other non-adhesive wear behavior [31]. While most of the tribological tests of polymer composites were conducted by adding short fiber and nanoparticles [32, 33], only a few reported in tribology regarding continuous fiber reinforcement. This was probably due to an immature manufacturing process. The introduction of the printed FDM technique in manufacturing enabled to lay down continuous fiber uniformly, providing stabilized structure objects.

Jian Li et al carried out the tribology experiment of fiber-polymer composites [34]. They reported that an addition of short carbon fiber content at a volume fraction of 20% in continuous carbon fiber composites could reduce the friction and wear rate [35]. Other researches related to sliding wear of short fiber-reinforced polymer composites were presented by Li et al [33], who reported the tribology performance of short fiber-

reinforced polymers (SFRP) with the addition of rigid nanoparticles. The load-carrying capacity of SFRP was mainly determined by the properties of fibers. With the addition of nanoparticles, adhesion between worn surface and counterpart, as well as stress concentration were reduced because of the production of 'roller effects' [32]. Li. C et al [32] proposed the wear sequence of fiber reinforced composites. The wear process of fiber-reinforced composites had 4 stages, shown in figure 5;

1. Polymer wear and fiber thinning.
2. Fiber fracture.
3. Fiber and polymer debonding.
4. Fiber removal.

Fiber debonding and fiber removal occurred simultaneously. A severed breakage of the polymer matrix resulted in a large fiber exposure. Eventually, the fiber was debonded and removed.

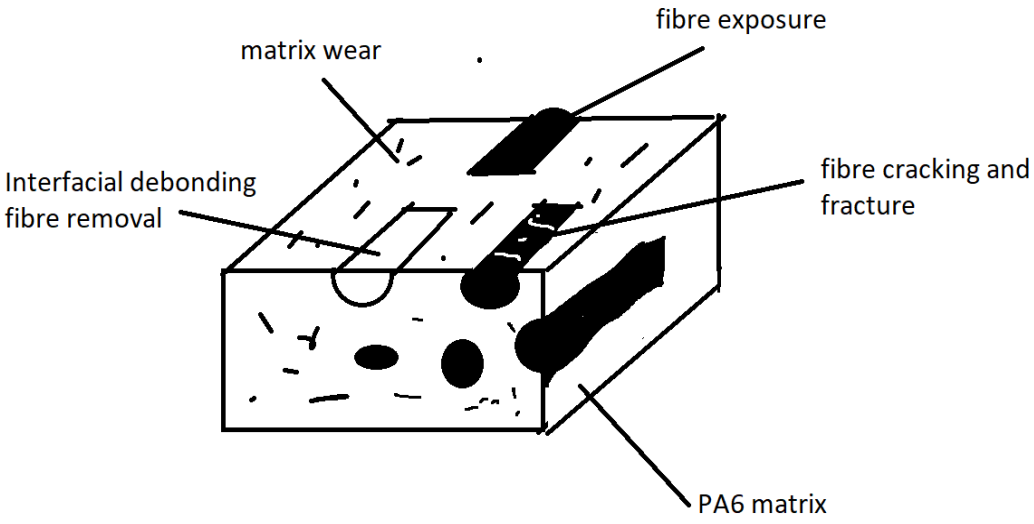

Figure 5. (a) Schematic demonstration of the wear process of carbon fiber reinforced composites. 1; Matrix wear - fiber thinning, 2; Fiber fracture, 3; Fiber and matrix debonding, 4, Fiber removal

Ming Luo et al investigated the tribology behavior of FDM printed short carbon fiber reinforced nylon composites (SCFRN) with surface textures under dry and water lubricated conditions [36]. He immersed the short carbon fiber nylon composites in water for tribology experiment. His results showed that SCFRN presented a low stable friction coefficient and a high specific wear rate under water lubricated condition. He then involved surface texture for further tribology experiment. Under a dry condition, surface texture did improve the wear resistance. However, surface texture provided little positive impact on improving the wear performance, probably due to the surface softening effect. By observing the SEM images, SCFRN showed a clean and smooth worn surface, less micro-sized grooves and fiber debris were observed.

2.4 Scratch experiment on polymer composites

Although wear surface can be analyzed to determine its damage mechanism through the tribology experiment, it cannot deduce how the fiber-polymer debris may affect the worn surface during the sliding progress. For example, Dasari A et al stated polymer debris formed a transfer film on the counterpart. Detached debris particles gave a three-body abrasive wear mechanism [37]. All these scenarios changed the composite worn surface due to wear. To further understand the composite wear characteristics and wear debris particles, scratching experiment is helpful

In the past few years researches were carrying out on the scratch performance of polymers due to the extended usage in many industries. Unlike metals, polymers are very sensitive to surface deformation and damage, even at low load condition. To evaluate the scratch performance, ISO [38] has standardized the testing procedure for scratch testing of polymers, where by controlling the force or displacement of a hard spherical tip to indent onto a polymer surface. After that, it moves across on it with a certain speed.

Two types of damage could be usually found in polymers in scratch-induced test: ductile damage and brittle damage. Researches showed that, mar, fish-scale, parabolic crack and polymer removal dominate the scratch damage mechanism on a polymer composites [40, 41, 42]. The scratch damage sequences can be categorized in four groups: strong-brittle, week-brittle, weak-ductile, strong-brittle, shown in figure 6.

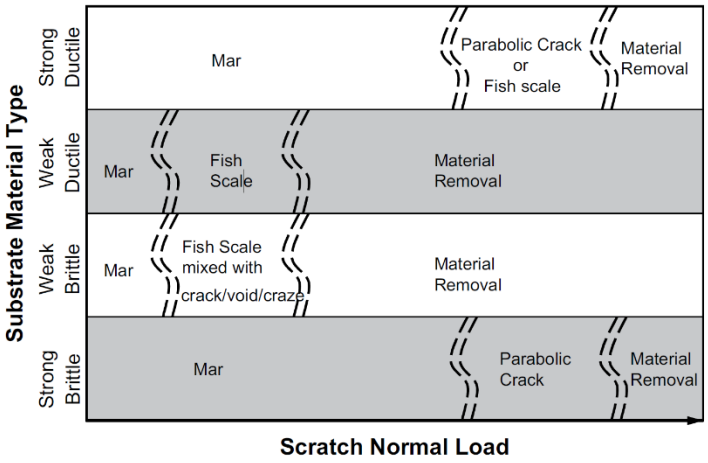

Figure 6. Material damage mechanism under different load [43].

The surface deformation of fiber reinforced composites is much complex than those of unreinforced polymer. Many researches focused on the scratch behaviors of fiber reinforced composites [44, 45, 46]. Mzali et al. presented the increase of normal load changed the wear mode from abrasive wear to fiber fracture, fiber pull-out and fiber extruded [45]. Qian C, et al investigated the effect of scratch behavior by adding short glass fiber. He found that the bulk mechanical properties of polybutylene terephthalate (PBT) were greatly improved, with the exception of the scratch resistance [45]. An addition of fiber caused a poor scratch resistance. The critical normal loads of material removal declined comparing with the neat PBT. In a large normal load, a severe surface damage was observed. The onset of material removal declined with the increasing fiber content [45].

2.5 Numerical analysis of scratch test.

With an improved computing capability, numerical analysis on scratch performance becomes feasible. Many researches focused on three dimensional FEM analysis [48,

49]. Despite FEM simulations still have a long way to model realistic polymer scratch behavior and accurate damage prediction, they are effective to visualize the stress distribution and initialized failure.

To investigate the scratch behavior of fiber reinforced polymer, there were attempts on simulating multiphase polymeric systems. This was much complex than single phase polymeric systems because the interaction between reinforce phase and matrix phase may trigger stress concentration and localized deformation [50]. By simply adding reinforced material as a second phase to increase strength and modulus of the composite did not improve scratch resistance [45, 52]. The scratch resistance was affected by reinforced material types, size, loading and shape. Further research on tribology performance of epoxy and styrene-acrylonitrile copolymer-based composites indicated that hard reinforcement filler increased scratch hardness while soft fillers decreased compressive yield stress [53]. Vijay Kisan et al showed that a larger volume fraction of reinforce particles posted an even distribution of stress across polymer's scratch region. A smaller reinforced particle size under the same volume fraction decreased the stress magnitude of debonding behind the scratch tip [50].

The FEM modeling in this thesis is to systematically investigate how the scratch parameters could affect the stress distribution of a fiber-composites specimen. This could effectively provide visualized information and linkage to the tribology and scratch experiment carried out in this thesis work, to explain the damage mechanism.

Chapter 3. Experimental Methodology

3.1 Materials properties and 3D printing progress

Two types of specimens are printed and tested.

- A nylon composites commercially named Onyx, a nylon filament that incorporates short carbon fibers. This is the short carbon fiber composites (SCFC).
- Continuous fiber reinforced composites (CCFC), nylon filament is the matrix, reinforced continuous carbon fibers

Properties	Nylon 6	Short carbon fiber (SCF/Onyx)	Continuous Carbon fiber
Tensile Strength (MPa)	51	36	800
Tensile Modulus (MPa)	1700	1400	60000
Flexural Strength (MPa)	50	81	540
Flexural Modulus (MPa)	1400	3600	51000

Table 1. Tensile and Flexural properties of nylon 6 filament, short carbon fiber filament and continuous fiber filament [55].

SCFC filament was in a diameter of 1.75mm and CCFC filament had a diameter of 0.35mm. They were both prefabricated in bundles (around 1000 fibers in each bundle), infused with a sizing agent, along with a certain volume fraction of nylon. The average length of short carbon fiber was approximately 100um. The density of short fiber bundle and continuous carbon bundle were 1.2g/cm^3 and 1.5g/cm^3, respectively. All filaments were stored in a Pelican 1430 dry box in order to minimize moisture

absorption prior testing [54]. The mechanical properties of nylon 6 and fibers are represented in Table 1 [55].

All neat nylon, SCFC and CCFC using in the thesis were printed by MarkForged Mark Two desktop 3D printer. This machine consisted of two print heads and extruders, enabling to print nylon and carbon fiber separately, shown in figure 7. One extruder used for printing nylon-SCF while another one was for carbon fiber. The sequence of the printer operates with fiber reinforced filament is described as follow:

- The nylon filament injector and fiber filament injector are heated up to 273℃ and 232℃, respectively.
- The filaments are pulled into their corresponding injector.
- Filaments are fused and printed on a printing bed with a temperature of 120℃, following the preset pattern.
- The filament is cooled down after laying up, obtaining the layer's final shape.
- Once the whole layer has finished the lay-up, the printing bed moves down, allowing the next layer to be printed.

The geometry of the specimen was designed by using SolidWorks software, followed by exporting as an STL file and importing to Mark Two desktop printer. Two types of fiber pattern could be selected in the printer: concentric and isotropic. This fiber pattern consisted of parallel lines, with or without fiber bundles. The 3D printer was driven by Eiger software. In default, fiber orientation was in 45-degree rotation for each layer but this setting could be manually modified to 0-degree. In this thesis, all carbon fiber reinforced bundles had a 0-degree fiber angle (in longitudinal direction) in both tensile and tribology experiments. The layer height was set to 0.125mm. The fiber bundles were prefabricated by Markforged company so the volume fraction of carbon fiber reinforced composites could not be changed.

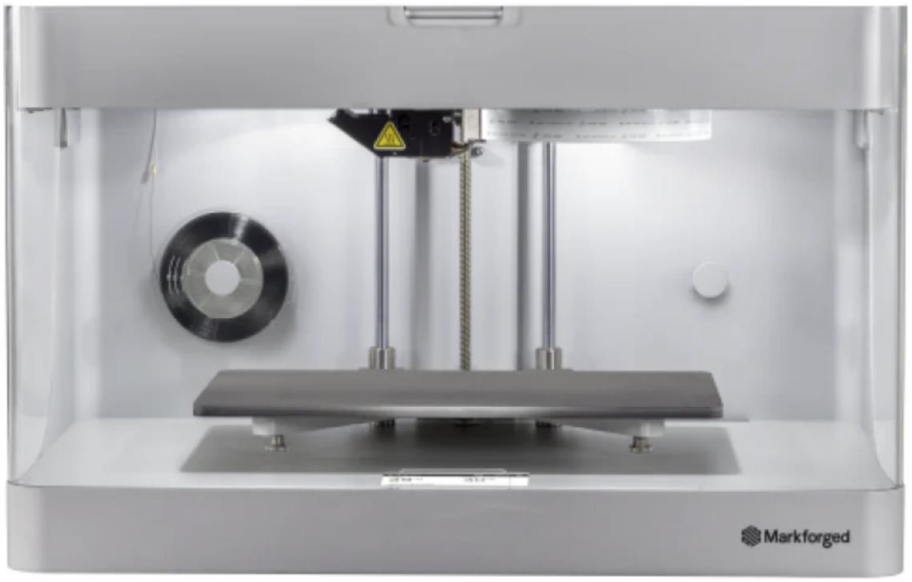

Figure 7. Front view of Mark Two printer

3.2 The procedures of moisturized and drying conditions

Two standards were usually implemented for moisture conditioning methods [56, 57].

- Immersed in water (at either room temperature or boiling water temperature)
- Exposure in air (temperatures from 23 to 70, relative humidity from 50 to 100%) [30]

The procedure followed the standard of ISO-1110. Compared with exposure in air, ISO-1110 dramatically speeds up the water absorption in nylon composites. However, over conditioning occurred [56] (more moisture could be absorbed under exposure in air). In this circumstance, the conditioning terminated after the moisture in nylon composites reached the saturation levels.

It should be noticed that the original condition (the condition in which the specimens were printed out from the Mark Two printer) was not investigated. The reason was that nylon and nylon composite easily absorbed moisture when they exposed in air. That means in original condition, there was a certain level of moisture within the specimens

already. In addition, the humidity in each testing condition greatly depended on the weather condition, which was not possible and pointless to control. Therefore, the procedure of testing the mechanical properties of the specimens of original condition were not considered.

3.3 Tensile test experiment setup

To investigate the influence of water absorption on the tensile properties of 3D printed composites, we selected two types of composites for the experiment, the neat nylon, SCFC and CCFC. Tensile experiments followed the standard – AS 1145.1-2001 (Australian Standard – Determination of tensile properties of plastics materials). The specimens were prepared with a dimension of 250mm in length 15mm in width 1mm in thickness. The centerline of the pattern had a minor section with a printing angle of 45-degree which was inevitable due to the default setting of the 3D printer. Each layer printing height was set to be 0.125mm therefore total 8 layers were printed.

The tensile test was divided into six categories. They were the SCFC under dry condition and immerse in water for 24 hours. the SCFC under dry condition and immerse in water for 24 hours, the CCFC under dry condition and immerse in water for 24 hours. At least three specimens for each category were tested for each test. Mass gains of the samples were recorded by Sartorius Ultra-Micro lab balances.

Based on ASTM D3039, tensile tests were carried out on a universal testing machine – Instron 5567 at a constant speed of 5mm/min. The gauge length with 50mm on each side was clamped by two pieces of aluminum adhered to both ends of all specimens by using ultra high strength epoxy adhesive. Each test was conducted until the specimen failed.

3.4 Tribology experiment

Pin-on-disk wear test was selected. Due to the Mark Two 3D desktop printer restriction, SCFC samples were printed in cylinder shape with a diameter of 5mm and height of 12mm, while the CCFC were manufactured in cube shape with a cross section area of 4mm X 5mm. Pin-on-disk tests were carried out by using NANOVEA(MT/60/NI) tribometer, shown in figure 8, with a period of 20 hours under 1MPa load and 0.5m/s sliding speed. The counterpart was a carbon steel disk (100Cr6) with a hardness of 13GPa [37]. The outer diameter of the carbon steel disk is 42mm while the inner diameter was 25mm. The disk was polished by grand paper P400 prior the tribology testing in order to get the surface roughness (Ra) of about 230nm. Before the wear test, the stainless steel counterpart was cleaned with ethanol and dried.

The samples with moisture absorption were prepared by immersing into water at 23^{O}C. To understand the effect of the moisture level on tribological properties of printed composites, two groups of samples were prepared by immersing the samples into water with different time duration, namely 24 and 240 hours.

Specimens used for tribology were initially dried in the oven with 60°C for 3 days after printing. After this stage was completed, the mass was recorded as M1. This was followed by fully immersing them in water with varied time, recording the mass as M2, and the moisture level of the sample was calculated as M2-M1. Tribology tests were carried out next. At last, specimens which completed the tests were placed in the oven again for 5 days. When this procedure was completed, the final mass was recorded as M3, the mass change, Δm, during the sliding wear was calculated as M3-M1.

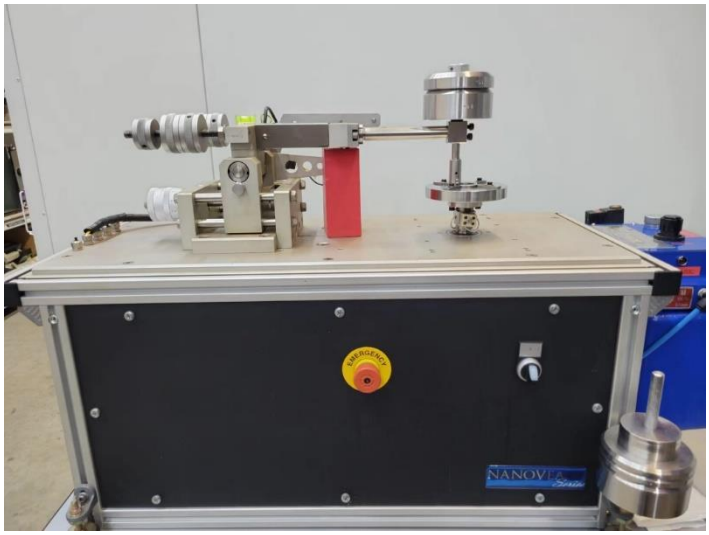

Figure 8. NANOVEA Tribometer

Friction coefficients were recorded by NANOVEA tribometer software implemented in computer. Specific wear rate of both short fiber composites and continuous fiber composites was calculated by the following equation [58]:

$$W = \frac{\Delta m}{\rho \times F_N \times L} \ [\frac{mm^3}{N \times m}]$$

where Δm was the mass loss of specimens during the test, ρ was density, Fn was the applied normal force and L was sliding distance.

3.5 FEM modeling

FEM study focused on the stress field development of a polymer-fiber composites. FEM modeling was created by using the finite element software ABAQUS to study the scratch deformation and stress development around the fiber. The numerical modeling was carried out by using a High Performance Computer. To reduce the simulation time, half-symmetric model of rigid tip scratching a polymer-fiber composite was selected. The scratch tip was a sphere, and it was assumed to be rigid, scratching along the direction as shown in figure 9. The scratch simulation follows the ASTM D7027

standard [59]. The finite element model in this work was created with a rectangular parallelepiped of $750 \times 100 \times 100$ μm^3. A representative volume element (RVE) was the smallest volume to that can be done to evaluate the structure, orientation and parameters of macroscopic model. The RVE was selected from a representative cross-sectional area shown in Fig.10, and the average diameter of carbon fiber was 10 μm. To investigate the scratch behavior on a composite material, several models were established with different fiber volume fraction, different scratch indenter radius. The first type was based on the experimental morphology, where carbon fibers are randomly distributed as per observation. The fiber volume fraction in the RVE was set to 3.1%, 6.2%, 19% and 38%. The type of model was established with carbon fibers evenly distributed. The fiber distribution with different fiber volume fraction was shown in figure 11.

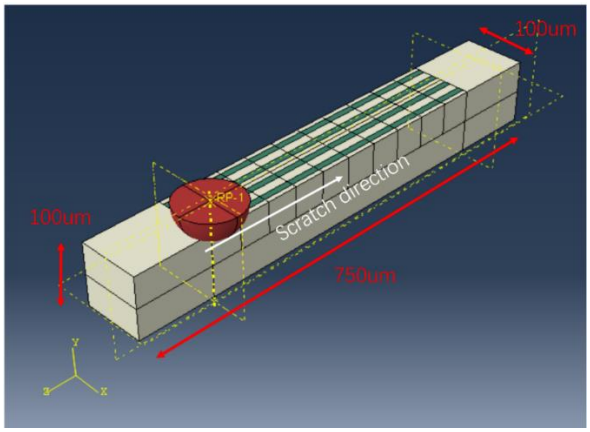

Figure 9. The dimension of FEM model.

The model is in half symmetric in order to reduce the time of simulation. The loading and boundary conditions were applied similarly to those in the experimental test. Specifically, the bottom surface of the model was constrained. The models were loaded using the rigid indenter by a downward force, increasing from 0 to 50 mN with different settings. Then the scratching starts with the indenter sliding along 400 μm under the peak force value. All material properties used in the FEM model are listed in Table 2. The material parameters were set based on the value obtained from the literature regarding the typical properties of nylon 6 and carbon fiber [28, 77].

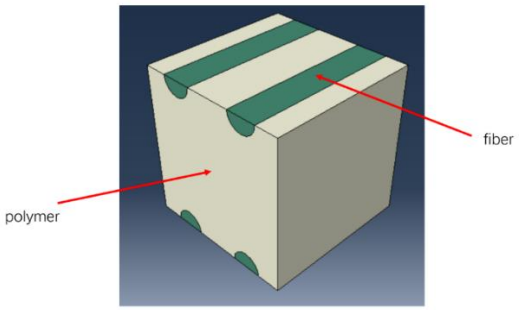

Figure 10. A RVE of fiber reinforced composites with volume fraction of fiber 6.3%

	Young's modulus (GPa)	Yield stress (MPa)	Poisson's ratio	Fracture strain	Density (g/cm3)	Strain hardening Slope (MPa)
Polymer	0.53	86	0.4	0.045	1.1	25
Fiber	150	2500	0.2	0.02	1.4	-

Table 2. FEM Simulation preset parameters.

The FE analysis was performed in Abaqus/Explicit code. In accordance with the work by Mzali et al, the matrix was meshed by using the solid continuum brick element (type: C3D8). The elemental size was set to be 5 μm. In total, the model consists of 46,000 solid continuum elements.

The surface-to-surface contact algorithm was considered to simulate the non-bonded part [23], where a frictional coefficient of 0.3 between the surface of indenter and matrix, and a friction coefficient of 0.1 between indenter and fiber were used in this work. The carbon fiber and nylon were both assumed as linear elastic isotropic material. The polymer matrix needs to be considered to be elastic-plastic. The Johnson-Cook model is involved to specify the hardening behavior and the strain-rate dependence of the yield stress. The plastic strain and stress relationship is shown as below:

$$\sigma = \left[A + B\left(\bar{\varepsilon}_{pl}\right)^{n}\right]\left[1 + C\ln\left(\frac{\dot{\bar{\varepsilon}}_{pl}}{\dot{\varepsilon}_{0}}\right)\right]$$

$\bar{\varepsilon}_{pl}$ is the equivalent plastic strain, $\bar{\varepsilon}_0$ and $\bar{\varepsilon}_{pl}$ are the strain rate and plastic strain rate. *A, B,* C, *n* are material constants. The temperature effect is not taken into account in this work. The relevant material properties of carbon fiber and nylon matrix were summarized in the table 2.

The interface between fiber-polymer was using a cohesive interaction. The damage profile is defined as traction-separation. It includes a linear elastic behavior and then, and plastic damage behavior [78]. The cohesive stiffness set in ABAQUS is 5 x 10^7 MPa. The plastic damage followed the quadratic nominal stress criterion for the initiation of delamination. Delamination growth once the crack is initiated. The fracture energy is set to be 0.01MJ/mm^2, according to other literature reporting the fiber reinforced composites [78]."

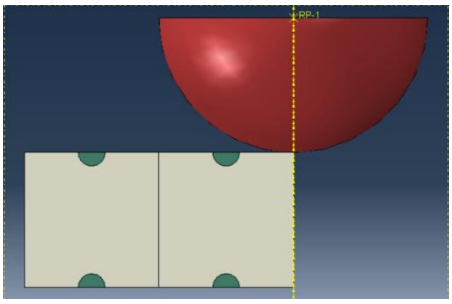

3.1 wt%

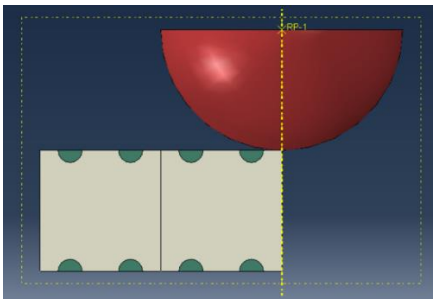

6.3 wt%

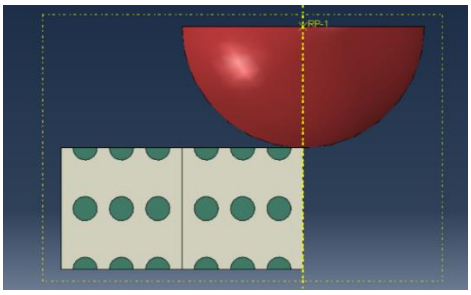

19 wt%

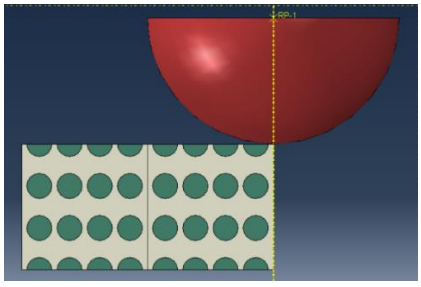

38 wt%

Figure 11. Fiber distribution of RVE with different volume fraction.

The FEM simulation can be divided into four categories for analysis. 1. The stress distribution of fiber-reinforced composites with different fiber volume fraction. 2.

Under the same volume fraction of fiber, the stress distribution with different load on the scratch indenter. 3. Under the same volume fraction, the stress distribution with a variation of indenter radius. 4. To simulate the moisturized condition of a fiber-reinforced composites, changing the material properties of polymer was carried out to obtain the stress distribution. With the help of simulation, a better understanding of the relationship between the fiber-reinforced composites scratch damage process and its stress distribution is obtained, summarized as a scratch damage evolution map.

3.6 Scratch experiment

The samples used in scratching study were pre-impregnated short carbon fiber reinforced polymer composites (SCFC) and continuous carbon fiber reinforced polymer composites (CCFC). The specimens had a cross section area of 5mm X 10mm for scratching. Before commencing the scratch test, specimens were all polished using silicon carbide grinding papers from 320 to 4000 grit. They would be further polished by a 0.3um alumina paste.

The scratch tests were carried out by using an ultra-micro indentation system (UMIS), provided by CSIRO Australia. A diamond conical indenter with 60℃ with a tip radius 5um had been used. The scratch length was set to be 300um and the normal load was constant. The scratch speed was set to be 30um/s at constant. The penetration depth and tangential force were recorded by depth sensors and piezoelectric dynamometer, respectively [60]. The experiment varied the normal load from 5mN to 20Mn. To observe the effectiveness and damage mechanism of fiber during the scratch test, indenter was selected to scratch over the composites surface at a location that closed to the fiber, along the fiber longitudinal direction. After finishing the scratching test, the composites surface was coating by cooper, then it was examined by using a scanning electron microscope (Zeiss Sigma HD) with a 5KV accelerating voltage.

Chapter 4. Effects of moisture conditioning on tensile properties of 3D printed fiber-polymer composites

4.1 Characteristics of neat nylon, SCFC and CCFC of absorbing water

Figure 12 is the mass change curve of SCFC and CCFC specimens immersed in water. The procedure of immersing water of specimens followed standard 'ISO-1110'. CCFC saturated at 6.5wt% moisture gain and SCFC saturated at 8wt% with different time periods. Neat nylon was able to absorb more than 10wt% of moisture to reach saturation. It is clear that neat nylon presented the fastest water absorption rate for 100hours water immersion. SCFC and CCFC had a similar water absorption rate.

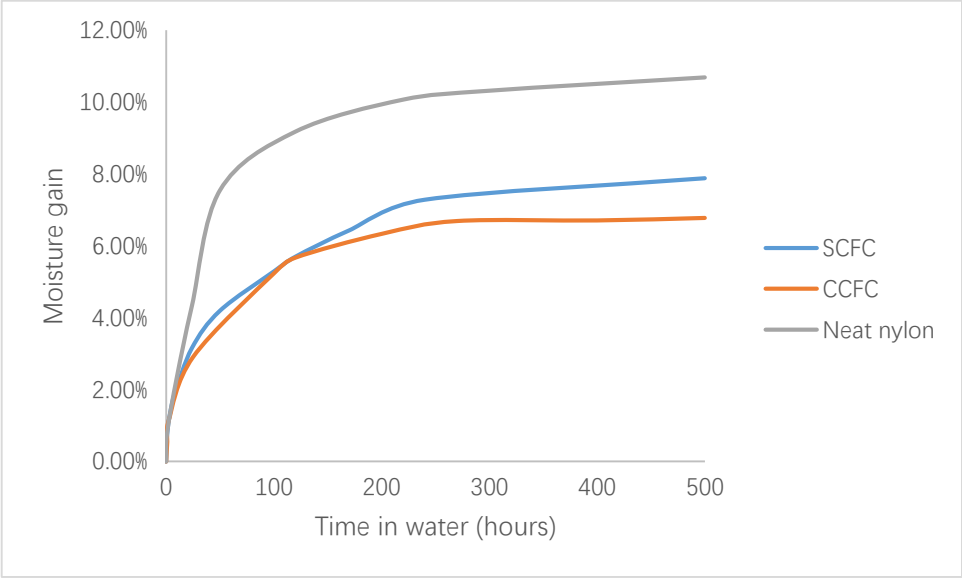

Figure 12. Mass change curve of specimens of neat nylon, SCFC and CCFC immersed in 23℃ water.

Compared with the results from literature [1, 29], the water absorption rates of all printed specimens were much faster than traditional fabricated methods. The literature showed up to 0.3 % mass gain for the conventionally manufactured neat nylon 6 under a water condition for 24 hours, or up to 0.25% for glass fiber epoxy resin composites (E-glass/PPS). The acceleration of water absorption rate could be attributed to the formation of voids and porosities in polymer specimens. Qinghao et al [24] used the

micro-CT technique to examine the voids and porosities content of FDM 3D printed samples were ranging from 10.3% to 14.3%, with an average value of 12.2 $\pm$ 0.9%. which showed that the void contents were much higher than the composites manufactured by traditional techniques. The latter were typically ranging from 0.02% to 5% for vacuum-assisted molding method [61]. The volume fraction of fiber in CCFC had an average volume fraction of 34$\pm$0.8%, and the fiber volume fraction of SCFC was around 12%, according to the previous work carried out by Qinghao et al [24]. The work by Qinghao et al also indicated that the voids volume fraction of CCFC was ranging from 10.3% to 14.3%, with the average being 12.2%, according to micro-CT presented in figure 13 [24]. In the region near the crack tip, large amount of voids provided a low resistance of crack growth. A large volume fraction of voids led to a poor stress transferring to fiber. Therefore, more debonding and fiber protruded.

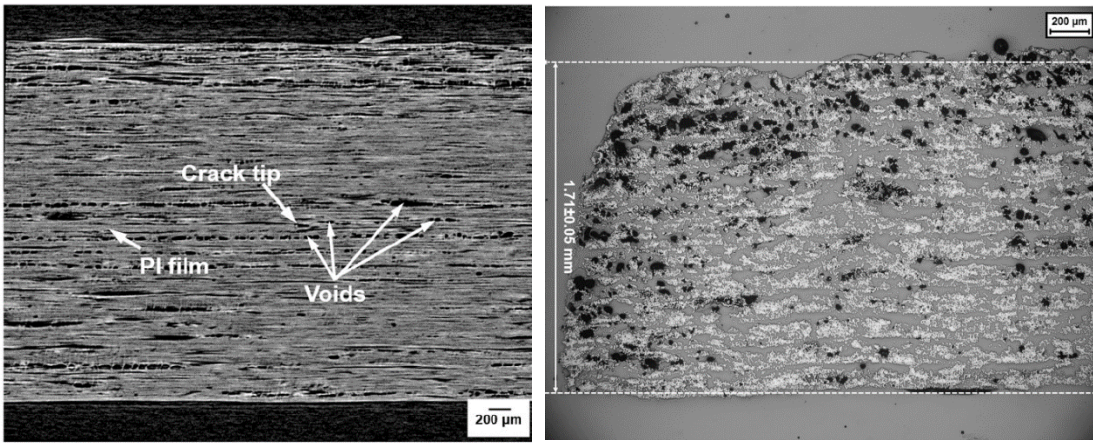

(a) (b)

Figure 13. Morphology of an additive manufacturing printed continuous fiber-nylon composites by micro-CT a) along Y axis. b) cross-section area [24].

Previous study reported that the existence of voids negatively affected the mechanical performance of printed carbon fiber reinforce composites (CFRC). The typical mechanical properties of carbon fiber and nylon 6 used were listed in table 3. The

theoretical tensile strength & modulus can be estimated using the rule of mixtures (RoM), which is shown in Equation 1:

$$E_c = V_f E_f + (1 - V_f) E_m$$

$$X_c = V_f X_f + (1 - V_f) X_m$$

V_f is the fiber volume fraction. E_f is the tensile modulus of fiber. E_m is the tensile modulus of polyamide 6. X_f is the tensile strength of fiber. X_m is the tensile strength of polyamide 6. The equation above is only valid for continuous fiber composites because the fiber length of CCFC was much larger than the critical length. To determine the yield strength and tensile modulus of short fiber composites. Equation 2 should be applied:

$$\sigma_{BC} = \tau_{Bi} \left(\frac{L}{D}\right) V_f + \sigma_{BM}(1 - V_f)$$

where τ_{Bi} is the shear stress between fiber and polyamide 6. L is the length of short fiber. D is the diameter of fiber.σ_{BM} is the strength of polyamide 6.

	Tensile strength (MPa)	Tensile modulus (GPa)
CF-T300-1K [28]	2500	150
Nylon	86	0.533

Table 3. Tensile properties of Neat nylon and carbon fiber [28, 77].

By using equation 1 and data from table 3, CCFC theoretical tensile strength and modulus should be 907MPa and 51.35GPa, respectively, which was still much higher than actual measured value. This could be explained by the existence of voids and porosities, which significantly affected the mechanical properties of CCFC.

Mechanical properties	Neat nylon	SCFC	CCFC
Tensile strength (MPa) in dry condition	20	28.4	531
Tensile modulus (MPa) in dry condition	441.8	946	27156
Tensile strength (MPa) in 24 hours water	13.1	23.23	474
Tensile modulus (MPa) in 24 hours water	300.6	681	24427

Table 4. Tensile properties of Neat nylon, SCFC and CCFC measured during tensile tests.

4.2 Tensile test results of 3D printed fiber reinforced composites under different moisture level

The stress strain curve of neat nylon 6, SCFC and CCFC under moisturized condition were illustrated in figure 14. Tensile strength and tensile modulus of neat nylon, SCFC and CCFC decreased with different percentage. In table 4, tensile strength and modulus of neat nylon decreased by all 33%, while SCFC decreased 19% and 28%, respectively. CCFC witnessed the least drop of tensile strength and modulus, at around 15%. In addition, the failure strain of SCFC under 24 hours' water condition decreased 50%.

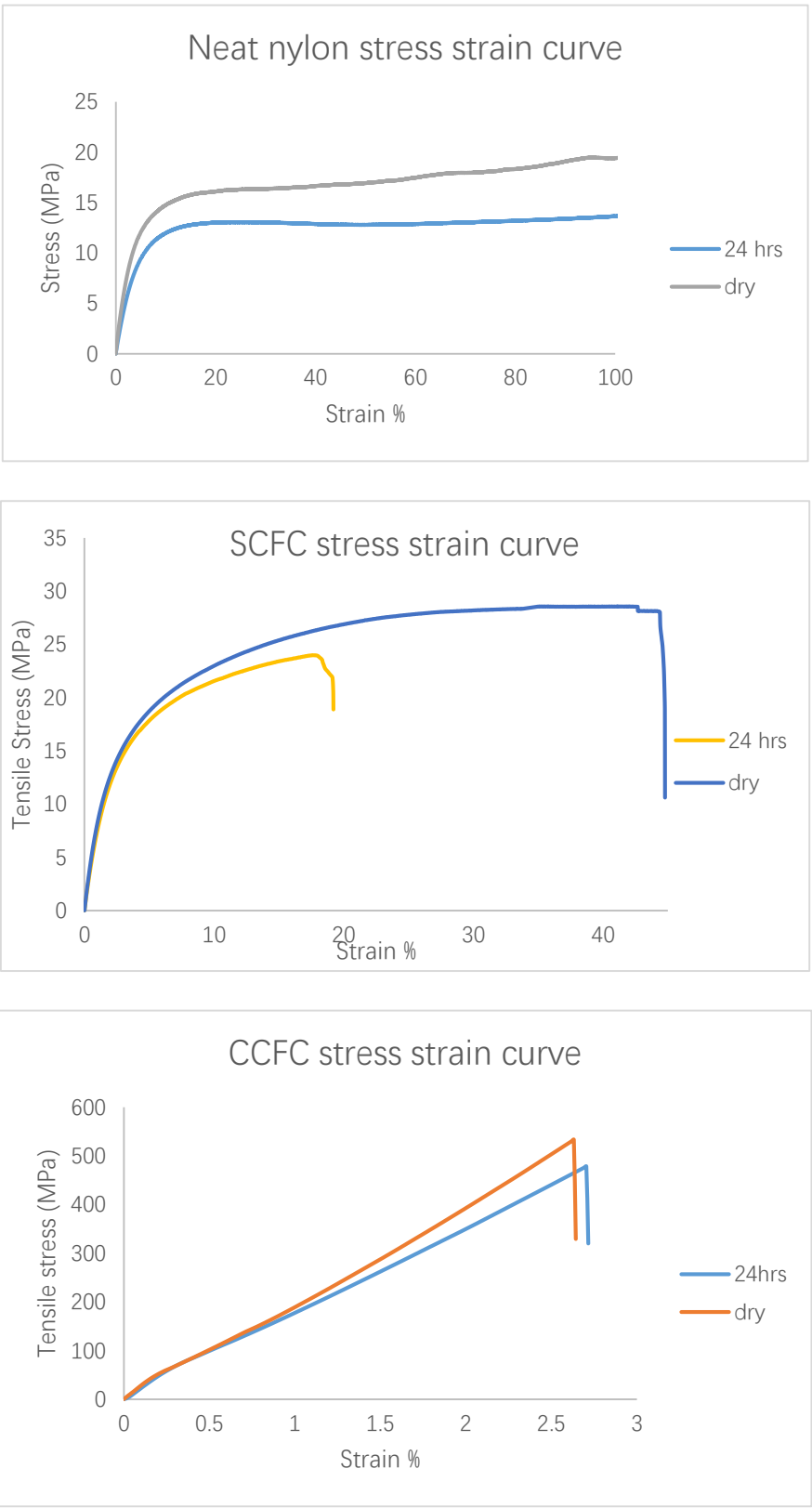

Figure 14. Stress strain curve of neat polyamide 6, SCFC and CCFC under dry and 24hours moisturized conditions.

4.3 Tensile stress between traditional molding method composites and FDM 3D printed composites under moisturized condition

The polymeric composites materials manufactured by traditional injected method in literature showed a drop of 10% of tensile strength for E-glass/PPS and carbon fiber 3k 2x2 Twill (indicated as T300) [29]. The decrease of tensile strength and modulus of SCFC were more significant in this work, at 20%.

	3D printed	Traditional molding
SCFC	-20%	-10 ~ 15%
CCFC	-11%	

Table 5. The drop of tensile properties under moisture condition between 3D printed composites and traditional molding manufacturing fiber composites [29].

There were more defects and voids produced during the SCFC printing process. Water was easy to be absorbed, especially in fiber-nylon interfacial region. This would particularly deteriorate the mechanical performance of SCFC specimens. Equation 2 is useable to explain the SCFC composite situation. As the bonding strength between fiber and nylon was getting weaker, the shear strength τ_{Bi} reduced. While the mechanical performance of nylon dropped because of the absorption of water, the whole sample failed and separated in boundary area, prior transferring more load to short fiber. This indicated short fiber did not maximize their role for reinforcement.

The water absorption posted a smaller effect on the tensile properties of CCFC, which was dropped by around 10%. There were two possible reasons. Firstly, it was because of the high volume fraction fiber in CCFC. When the volume fraction was high enough, and the fiber length was much greater than the critical length, the tensile strength of the composites was more dominated by fiber fibers, i.e. $\sigma_C \approx V_f \sigma_f$. Thus, continuous fiber tensile strength dominated the tensile strength of CCFC specimens, which is little affected by water absorption in polymer matrix. Secondly, the tensile tests were carried

out aligned in fiber direction. In this case, continuous fiber tightened the specimens all together in longitudinal direction. Even though the nylon became weak and failed during the tensile test, continuous fiber took most of the load.

4.4 An analysis of the strain behavior under water condition

According to figure 14, the stress-strain diagram of SCFC and CCFC shows different patterns. SCFC stress strain diagram was in a curve shape, while the CCFC presented a linear relationship. This indicated the changes in fracture mechanism of SCFC due to the low bonding strength. Initially, fiber took the loading until it reached the critical shear strength between fiber and nylon. Once the shear stress exceeded the critical value, short fibers were pulled-out from the nylon matrix. The stress-strain curve became flat. SCFC samples were no longer capable to take any more load, instead, it kept elongating until it broke. Under a moisturized condition, because of the weaker bonding strength between fiber-nylon region, fibers were easier to pull out. That was why the strain of a moisturized SCFC was much lower than SCFC in dry condition.

CCFC stress-strain curve showed different characteristics. As all the loads were transferred from nylon to continuous fiber, failure of the composites occurred with fiber fracture. The debonding of fiber-polymer posted less effects on the overall CCFC tensile performance.

Although it has been well known that the moisture in polymer or polyamides acts like a plasticizer, increasing its ductility [56], SCFC samples showed a great drop of its ductility. This was consistent with the results shown in literature [29]. The reduction of ductility in additive manufacturing could be attributed to the voids in the fiber – polymer bonding region. When SCFC was under water absorbed condition, the polymer part was easier to be elongated, acting like a plasticizer. It was easier to deformed towards two ends. While the deformation occurred between fiber and polymer was

greater due to the absorption of water, stress mismatch and concentration occurred in the region between fiber and polymer. Cracks and debonding were likely to form in fiber-nylon interfacial area. At the same time, the prefabricated carbon fiber bundle in the short carbon fiber – nylon filament compacted in radial direction during the fabrication process. Re-melting of fiber - polymer filament when it went through the nozzle allowed the carbon fiber bundle to relax in the radial direction, which expanding the entrapped tiny voids in the filament [24, 63]. These formation of voids deteriorated the strength of bonding and accelerated the crack formed in the bonding region. Therefore, SCFC specimen was brittle comparing to the neat polymer. CCFC's ductility did not show a noticeable difference.

4.5. Fractography analysis of tensile test samples.

To further investigate the damage mechanism of water absorbed composites, SEM analysis on the fracture surface of tensile test sample was carried out. Figure 15 presented the SEM on the fracture surface of CCFC under dry and moisturized conditions. It can be seen that there was a difference of damage mechanism. In the dry condition, the fracture cross section area microstructure showed fiber broken directly, while nylon was still attached with continuous fiber. Fibers were broken in clusters and bundles. A few fibers were extruded and failed individually. According to Ramesh et al [20], fiber failed in larger clusters can experience a high tensile stress.

On the other hand, bridging and hollow sections of nylon were observed for the samples immersed in water, shown in figure 15c. This indicated a poor bonding between fiber and nylon after they absorbed water. When absorbing water, nylon became soft and resulted in a weak mechanical performance. When tension was applied to the specimen, nylon was difficult to adhere with fibers, and debonding can easily occurred. This resulted in the separation of fiber bundles and clusters as nylon no longer tightened the fibers together, circled in figure 15d. From the work mentioned by Ramesh et al [20],

a separation of fiber bundles led to fiber broken singly, which can only experience a low tension. Therefore, the tensile strength of water absorbed specimens reduced.

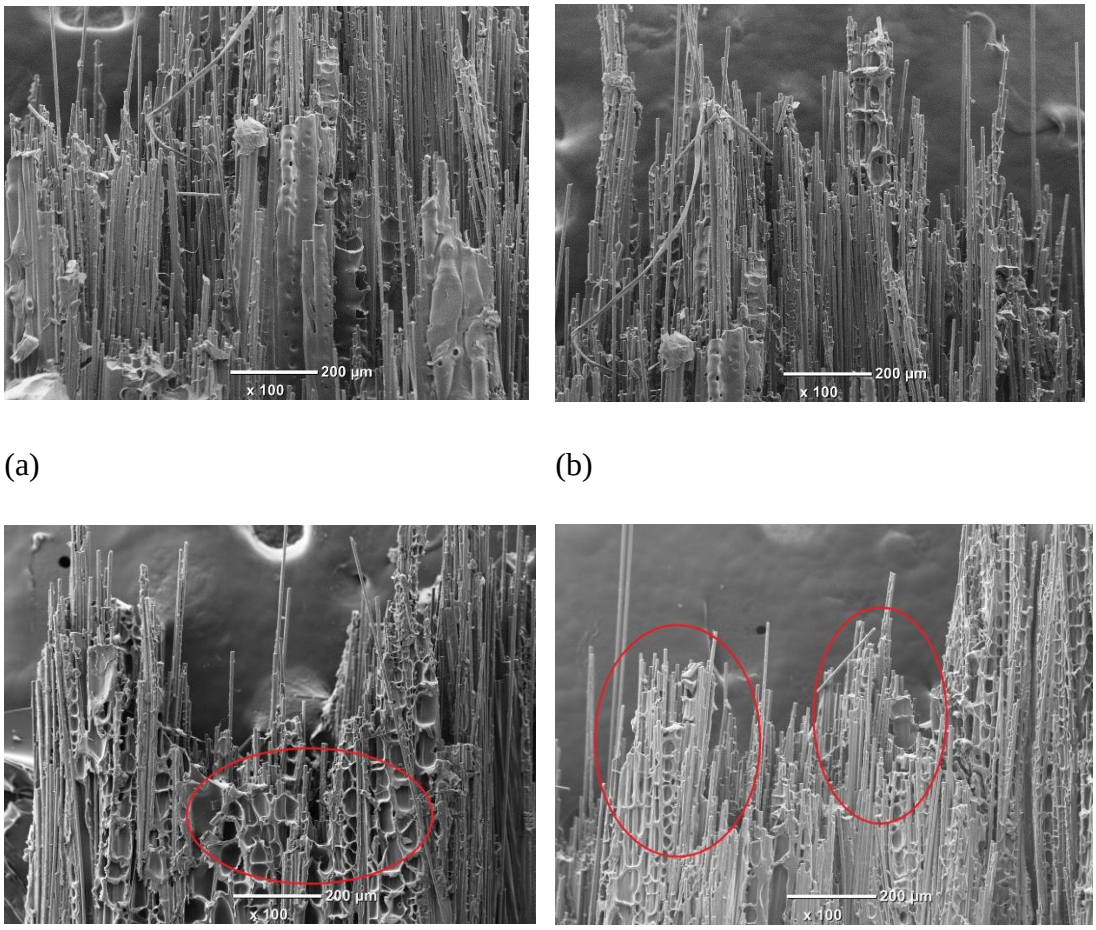

(a) (b)

(c) (d)

Figure 15. SEM of the breakage cross sectional area of CCFC. (a) and (b), under dry condition. (c) and (d),24 hours' water immersion condition.

Chapter 5. The wear performance and surface damage mechanism of tribology experiment under a moisturized condition

5.1 Wear behavior and damage mechanism under dry condition of SCFC and CCFC

Figure 16 represents the friction coefficients of SCFC and CCFC in dry conditions. The mean friction coefficient at steady stage for SCFC was about 0.3, and it was 0.45 for CCFC. The low friction coefficient of SCFC can be explained by the lower strength of polymer matrix due to water absorption. Polymer showed a poor mechanical strength performance [64]. Polymer debris can be easily peeled off to the sliding counterpart to form a transfer layer [65, 66]. The nylon matrix peeling off from the worn surface could also lead to short fiber extrusion, which accelerates the fiber removal and the formation of fiber debris. After that, the fiber debris which was trapped between transfer film and worn surface induced a three-body abrasive wear, changing the contact mode from wear surface – stainless steel counterpart to wear surface – fiber debris – transfer film [67, 68]. In this case, friction force is dependent of adhesion force between transfer film and the specimen, which is greatly dependent on the yield strength of polymer matrix. Therefore, the friction coefficient of SCFC was decreased with water absorption.

Figure 17 represents the specific wear rates of SCFC and CCFC in dry conditions. The wear rate of CCFC was about 30% lower than SCFC. CCFC should achieve a lower specific wear rate than SCFC because of a higher fiber volume fraction. Under the same load condition, each unit length of fiber of CCFC could take a lower load [69], taking most of the load during the wear process, protecting the matrix [33, 71].

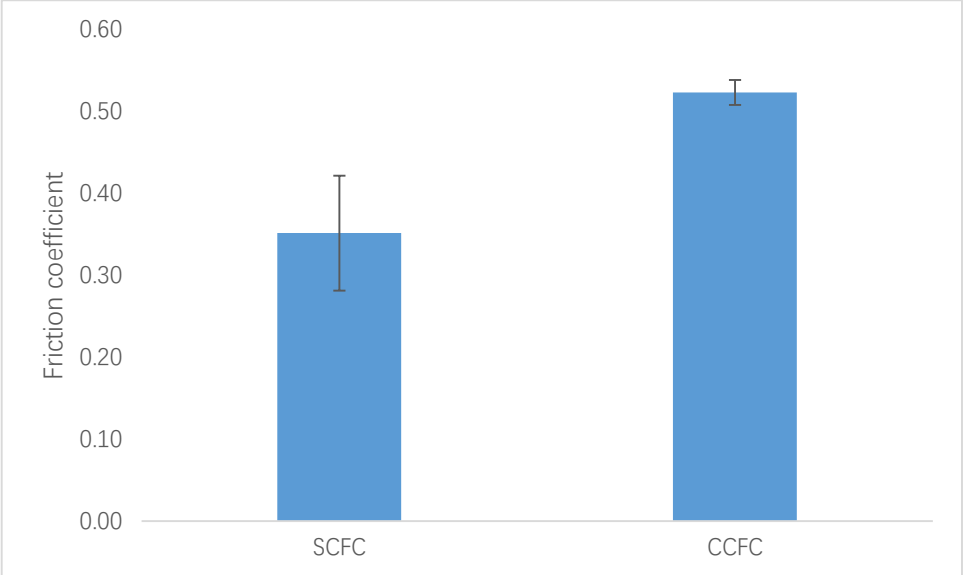

Figure 16. Coefficient of friction of SCFC and CCFC in dry conditions.

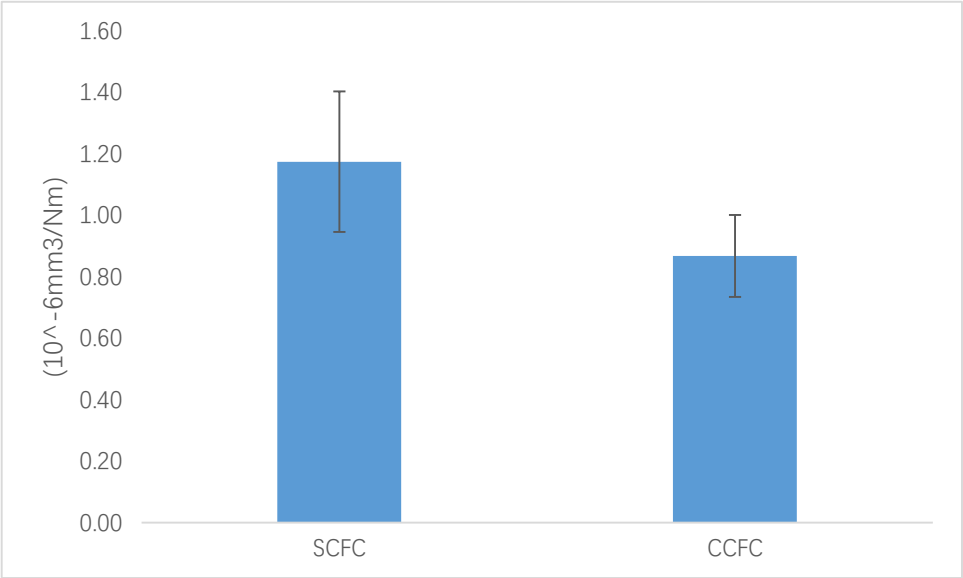

Figure 17. Specific wear rate of SCFC and CCFC in dry conditions.

Fiber volume affected the average unit length of fiber to take load. A large fiber volume fraction reduced the load taken by the unit length of fiber. This resulted in less affecting the fiber-nylon interface, giving less matrix damage. Also, there was less fiber pull out due to the well protection of matrix. This led to a low wear rate. In addition, carbon

fiber provided solid lubricating function [68, 72]. Carbon fiber is a graphitized carbon with hexagonal planes. During the tribology test, carbon fiber debris could decomposed into graphite crystals. The debris of carbon fiber formed a thin transfer film on the counterpart. This provided lubrication effect and it reduced the abrasive process [72].

The standard deviation specific wear rate of SCFC was higher than CCFC. There were two reasons. Firstly, it was because of the random distribution of short carbon distribution in filament, depending on the prefabricated process by 3D printer manufacturer. If the content of short fiber was higher in a particular section of filament, the printed part by using this section of filament would have a greater mechanical property, including the wear performance. Secondly, the existence of voids in SCFC samples posted a great effect on wear resistance. Voids were formed during the filament prefabrication and nozzle printing layout. The progress of generating voids was random. These two random factors may explain why there was a higher standard deviation for the SCFC wear samples.

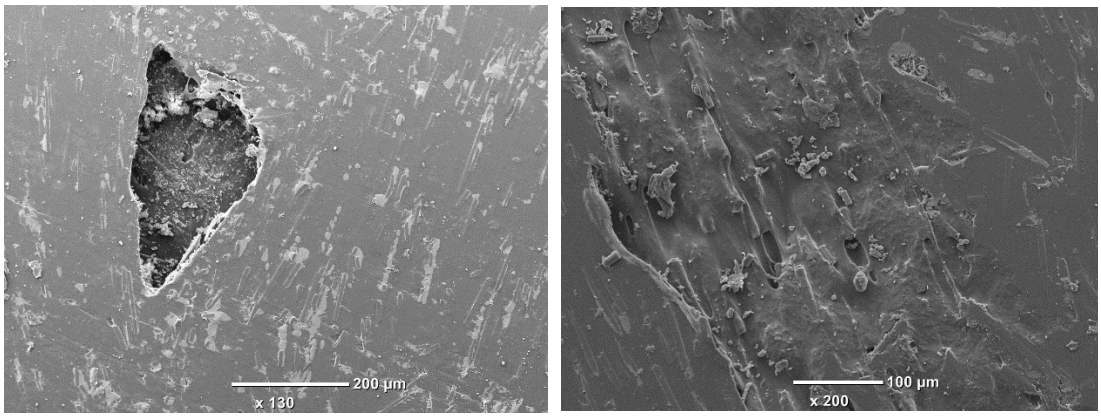

(a) (b)

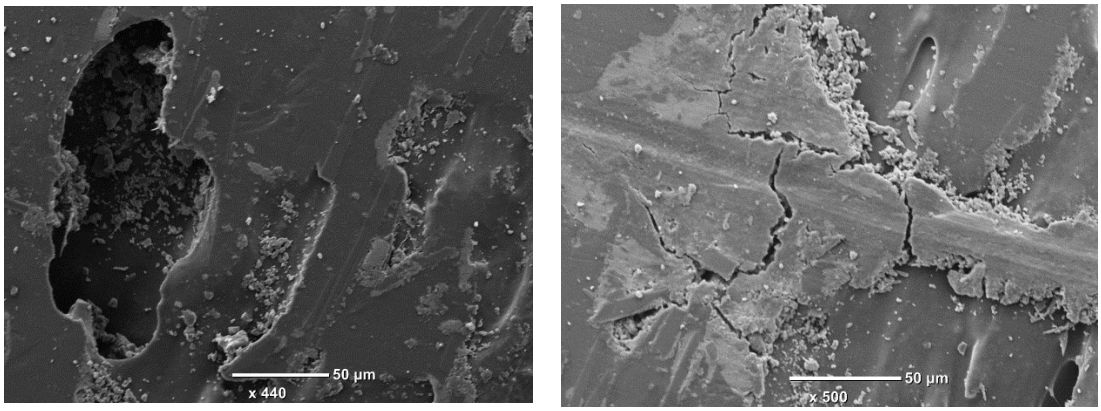

(c) (d)

Figure 18. SEM worn surface of SCFC in dry conditions.

The SEM images of short and continuous fiber composites wear surface were shown in figure 18 and 19. The results showed that the worn surface of SCFC was relatively smooth. In general, the wear grooves were shallow and the quality of worn surface remained intact.

The damage mechanisms for the dry specimen could be classified into four steps/types. They were polymer debris forming, fiber shifting, fiber breaking and fiber removing. Before the initialization of fiber damage, polymer broke into debris, then fiber shifting occurred due to less fiber – polymer bonding strength. Some fiber was pushed downward or away from its original position, while a very small portion of fiber was completely removed from worn surface. The fiber shifting process should occur simultaneously when the polymer was crushed into small debris as fiber was extruded out from the worn surface. Fiber remained and on the worn surface were compressed and broken into small pieces by the stainless steel sliding counterpart.

Figure 19 presents the SEM images of the worn surfaces of dry condition of CCFC. There was no polymer debris on the wear surface. Instead, fiber breakage and fiber removal were observed. This was because fiber took most of the load [64], confirming that there were more cracks and exfoliations in the fiber sections. When the counterpart scratched over the composites, fiber was compressed downward instead of pushing

sideway or pulling outward. In this case, the primary failure mode of fiber was fiber breakage and compressing.

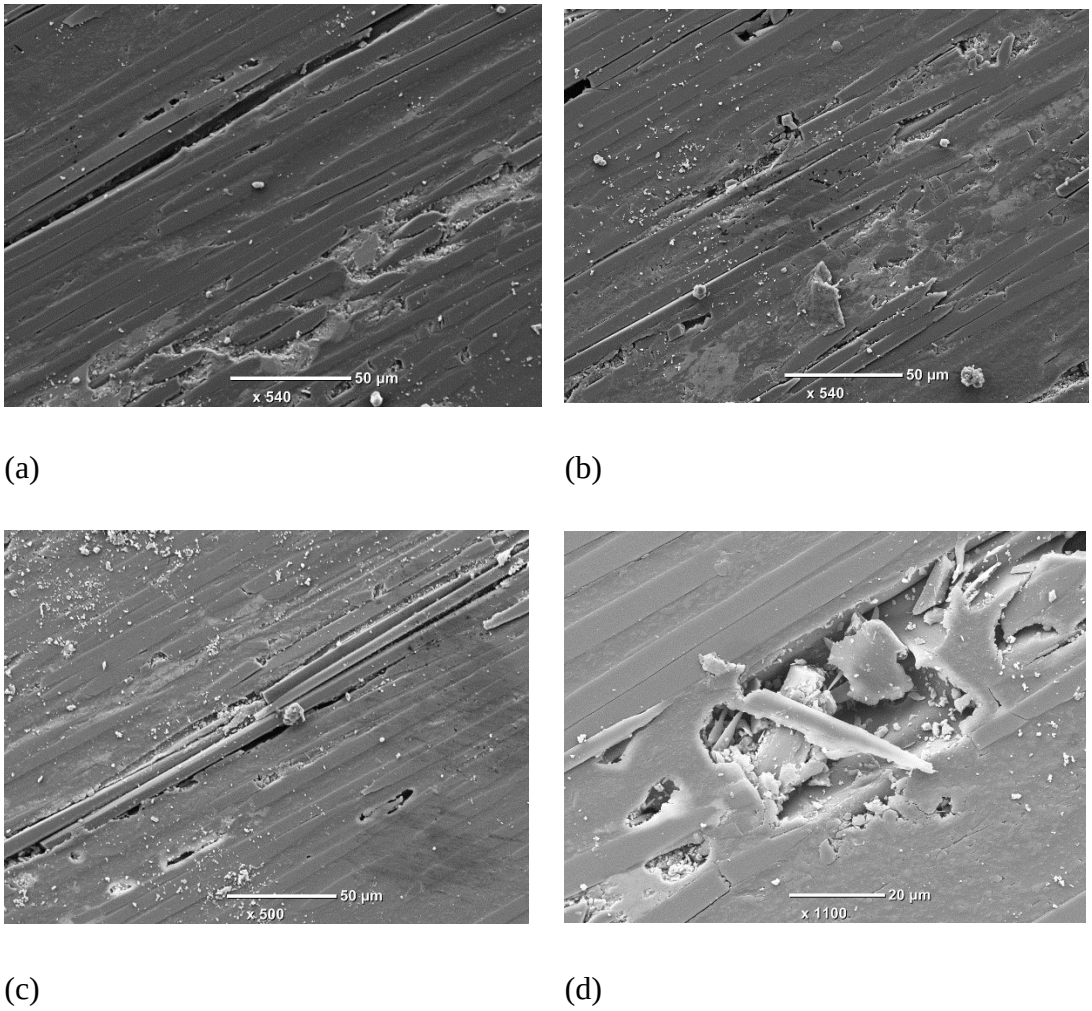

(a) (b)

(c) (d)

Figure 19. SEM worn surface of CCFC in dry conditions.

5.2 Wear behavior of moisturized SCFC.

Figure 20 compares the friction coefficient of SCFC composites from dry condition to immersing in water for 240hours. The applied load and sliding speed were 1MPa and 2MPa, 0.5 m/s, respectively. Figure 22 gives the specific wear rates of SCFC reinforced composites in different levels at different loadings. Under 1MPa load, the friction

coefficient raised as the SCFC composites contain an increasing amount of moisture. When the specimens immersed in water for 240hours, SCFC exhibited a high friction coefficient, which was around 0.7. When sliding with a soft worn surface condition, the friction layer on the surface would be subjected to plastic or viscoelastic deformation [74]. Although moisture trapped inside the SCFC acted as the coolant and lubricant during sliding [36], it couldn't fully offset the negative effect of reduction of polymer yield strength. The friction coefficient was determined by the real contact area of wear surface-counterpart and the shear strength of the sliding samples [75]. When polymer absorbed water, the yield strength decreased. Because the stress at the real contact area could be extremely high, a low yielding strength of polymer increased the real contact area due to the plastic deformation. The raise of true contact area could contribute to the increased friction coefficient. When the load increased to 2MPa, friction coefficient of SCFC dropped under a 240hours water condition, probably due to the change of wear mechanism because of the lubricating effect of moisture.

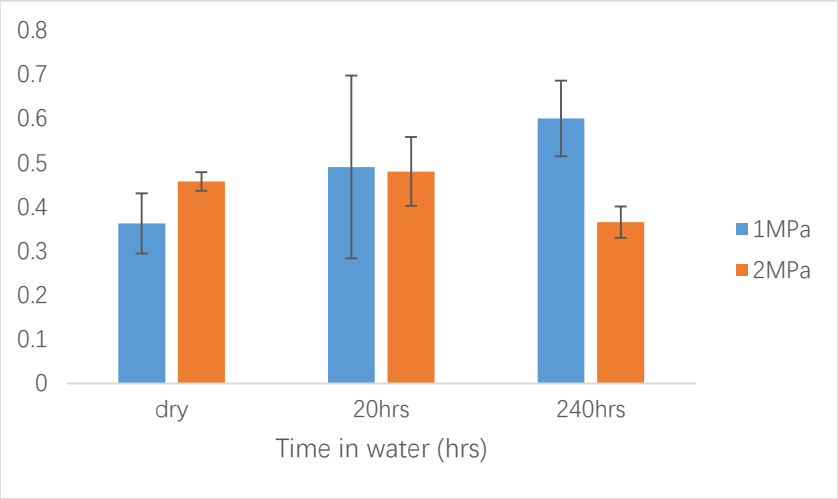

Figure 20. Coefficient of friction for different levels of moisture of SCFC under different loads

SCFC composites greatly deteriorated the wear resistance under moisturized conditions. The increase of moisture absorption resulted in a linear increase of the wear rate for

both 1MPa and 2MPa loads (Fig. 21). Compared with SCFC under dry condition, immersing in water for 240hours raised the wear rate 6 times. It was deemed that the high abrasive wear was an important factor for the high wear rate of the moisturized composites. This is because the softening effect of moisturized polymer enabled a large section of polymer was removed from the wear surface. Another possible explanation of high wear rate of water absorbed SCFC was the water effect. Moisture trapped inside the sample was released during sliding and it cleaned the debris away from the contact region [36]. In this case, it was difficult to reduce the adhesive wear. Therefore, these two factors dramatically led to a high wear rate of moisturized SCFC.

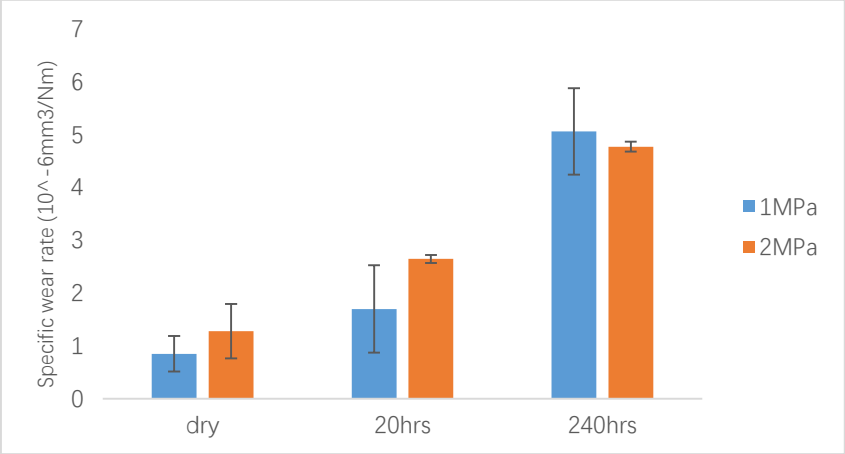

Figure 21. Specific wear rate for different levels of moisture of SCFC at different loads

Figure 22 shows the SEM of SCFC specimens with different times in water at 1MPa loading. Under dry sliding condition, some plowing marks were observed from the worn surfaces and the surface is relatively smooth. Not many fiber detachments or breakage on the worn surface were observed. In figure 22b, instead of completely removing from the surface, a few fibers were pushed sideway according to the sliding direction.

As the moisture level increased to 2wt%, immersing in water for 20 hours, the worn surface and wear mechanism had changed. Instead of smooth grooves on the wear surface, large section of polymer debris was formed during sliding, see in figure 22e & f. At the same time, cracking of fiber - polymer, fiber breakage, and fiber crushing were observed on the worn surface. This could attribute to the weakened surface mechanical strength of nylon [76]. The weakened nylon deteriorated the wear performance in several ways. Polymer debris was easily detached and fiber was likely to extruded from the surface. All these increased the probability of fiber removal. The probability of fiber removal also increased when cracks were formed between fiber and polymer, which is a typical failure mode under the weak bonding condition. Fiber breakage and fracture resulted in each unit length of fiber took a larger load, and it induced stress concentration. For those moisture level of SCFC for more than 7wt%. SCFC specimens were in saturation condition, and the worn surface damage was extremely severe. Large pieces of polymer surface were pulled off from the wear surface. At the same time, fiber extrusion was also observed. The protuberance-like deformation was an indication of severe stress concentration occurring on individual carbon fiber ends due to the distinctly different modulus of the fibers and the polymer [70]. However, there was slight cracking formation of the boundary between fiber and polymer. Fiber breakages on top the worn surface were not commonly observed. This could be attributed by the extremely poor mechanical strength of polymer. When the polymer acted like a plasticizer in a moisturized condition, large polymer sections containing fiber were pulled off before individual fibers were removed from the worn surface [1]. This was why the wear rate of SCFC with high moisture level was extremely high.

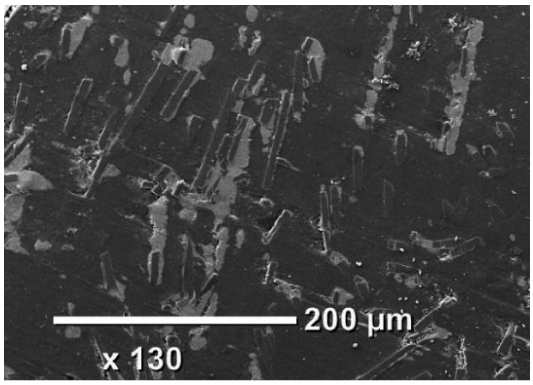

(a)

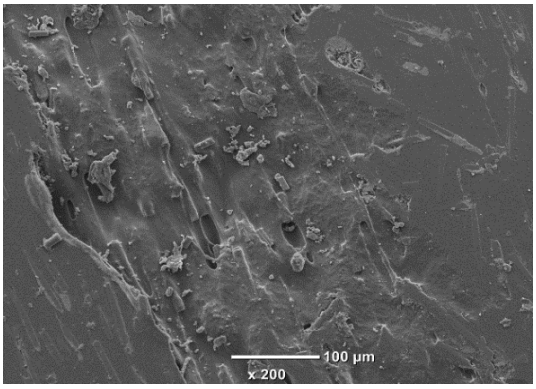

(b)

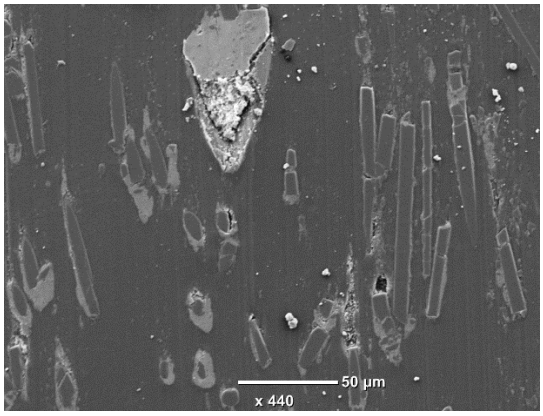

(c)

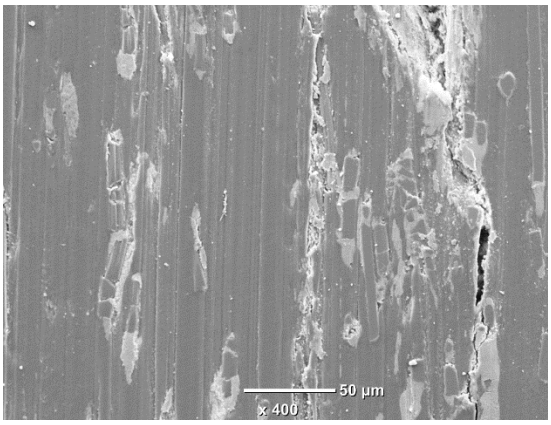

(d)

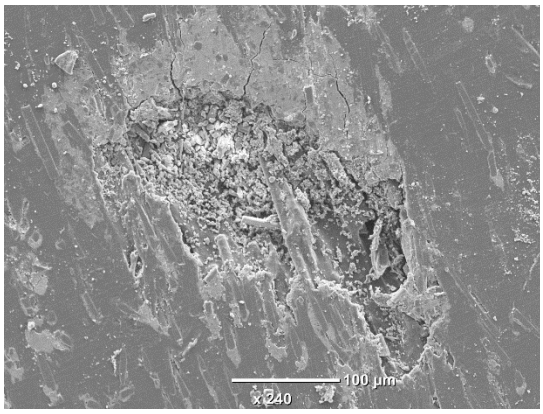

(e)

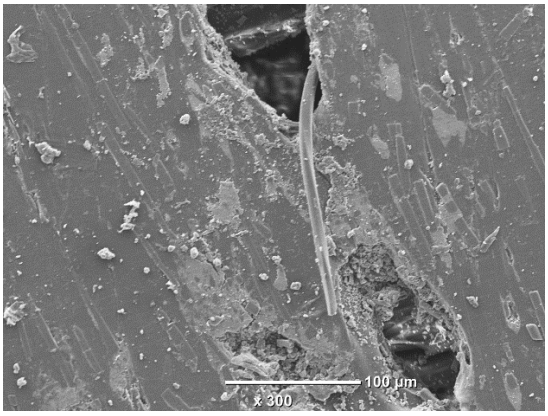

(f)

Figure 22. SEM of the worn surfaces of SCFC at different moisture. (a & b) under dry conditions (c & d) Under 20hours water condition; (e & f) Under 240hours water condition

5.3 Moisturized CCFC worn behavior analysis.

Figure 23 represents the coefficient of CCFC with different moisture levels at 1 and 2MPa. The friction coefficient dropped while the moisture level increased in both loading conditions. Compared with dry sliding conditions, coefficient of friction reduced from 0.5 to 0.35 at 240hours water conditions at 1MPa loading conditions, while it dropped from 0.6 to 0.45 at 2MPa loading conditions. The friction coefficient showed a different result from that of SCFC. This can be attributed to the effect of moisture lubrication, which can reduce the friction. Looking at the wear rate in figure 24, it showed that the specific wear rate of CCFC under moisturized condition decreased as well, especially for the case of 1MPa loading conditions. This indicated that moisture did not provide a negative impact on the wear performance of CCFC. Water in CCFC provided a great degree of lubricating effect and friction-induced thermal could be inhibited in aqueous environment [62]. Water cleaning the debris did not affect the wear behavior as continuous fiber in CCFC dominated the wear mechanism. Each unit length of fiber took a small amount of load, making the fiber not easy to fail. However, the trend of wear rate of CCFC under 2MPa showed different results. The lowest wear rate was observed when the specimens immersed in water for 20hours, while the wear rate in dry and 240hours conditions was similar. The change of the trend of the specific wear rate under different loading situation indicated that the wear mechanism has changed under a high load condition. This was probably due to the fact that the high loading caused more debris formation, which results in severed abrasion.

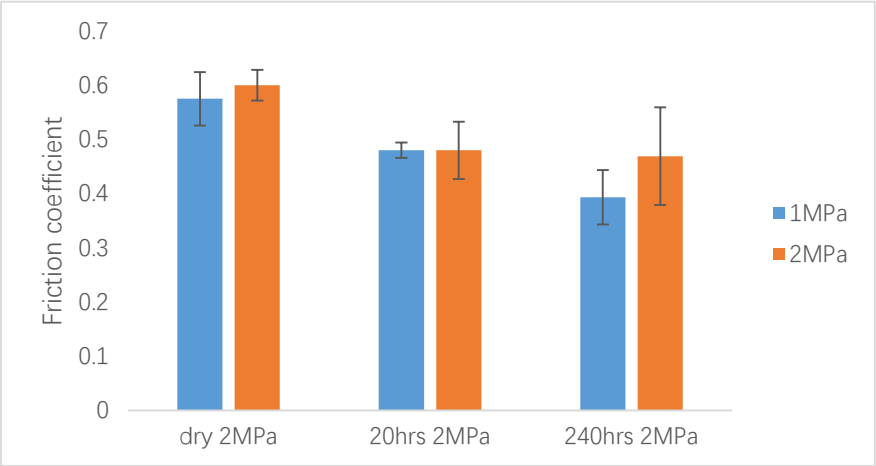

Figure 23. Coefficient of friction of CCFC with different moisture levels.

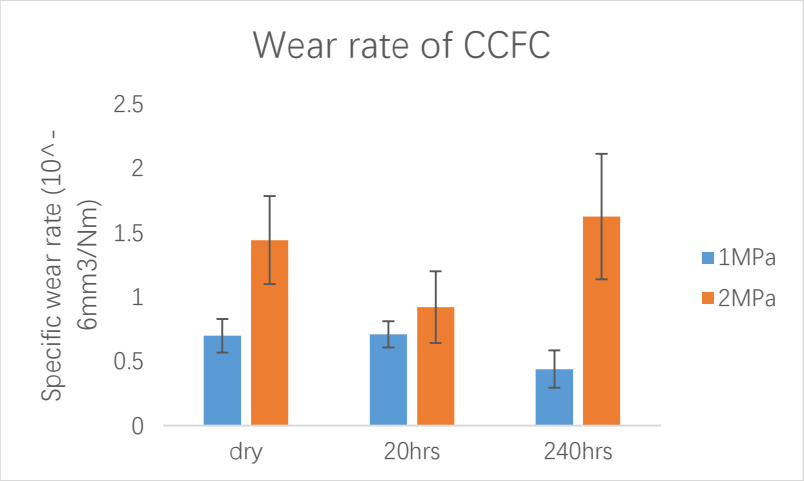

Figure 24. Specific wear rate of CCFC with different moisture levels.

Figure 25 compares SEM worn surface of CCFC composites subjected to different moisture levels at 0.5m/s and 1MPa condition. Under the dry condition, most common phenomenon was fiber breakage in worn surface, shown in figure 25a & b. Most of the carbon fiber was stick on top of the worn surface but broke into small pieces. This indicated that the bonding between fiber and polymer was strong enough to against counterpart sliding. Meanwhile, we can observe the polymer debris was stick with the continuous fiber, in figure 25a. This was due to the high contact temperature in this area. Polymer matrix was melted during sliding and stick with the nylon and counterpart.

It induced the adhesive wear mechanism during the sliding progress. This could explain why the coefficient friction of CCFC in dry condition was higher. Also, the adhesive-abrasive wear resulted in a high wear rate because of the high contact temperature and concentration of adhesive force. When CCFC absorbed water for 20 hours, tremendous fibers extrusion was observed. This implied that before the fiber extruded occurred, polymer was detached from the worn surface. The wear progress of CCFC under 20 hours condition would be polymer detachment, fiber extrusion and fiber shifting [8]. Looking at figure 25c & d, fiber thinning was not observed. Instead, fibers were pushed sideway along with the sliding direction. This can be explained by the decreased bonding strength between fiber and polymer after immersed in water. Fibers were slipped sideway or downward before they were thinning by asperity on counterpart. Fibers slipped sideway or removed were trapped between the worn surface and steel sliding counterpart, acting like the rollers. The 'rollers' played as a three-body wear mechanism, introducing the three-body abrasive wear during sliding. Therefore, this could explain why the friction coefficient and wear rate were lower comparing with the dry condition sliding. Figure 25e & f showed the CCFC worn surface under 240 hours' water situation. The worn surface was relatively smooth. The main worn characteristics were polymer deformation and fiber removal. Some cracks were found between the fiber and polymer. Only minor abrasive grooves were observed. This indicated the wear progress was polymer deformation, followed by boundary cracking, and eventually, fiber removal. The moisture lubricating and cleaning effect of water absorbed resulted in this wear progress [36].

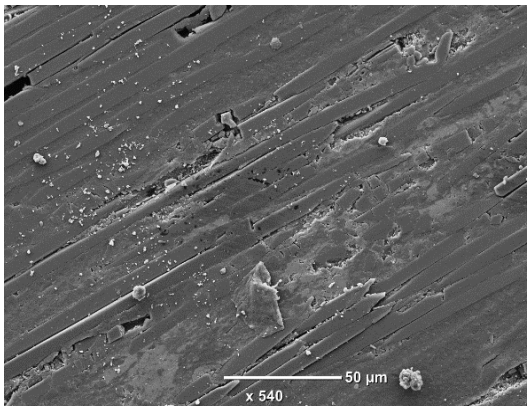

(a)

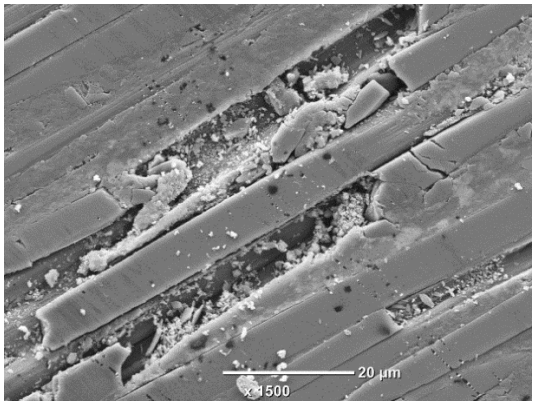

(b)

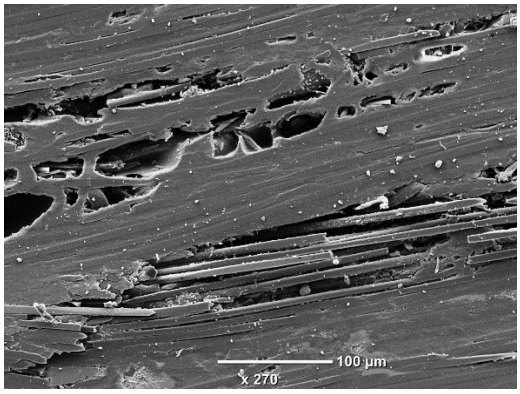

(c)

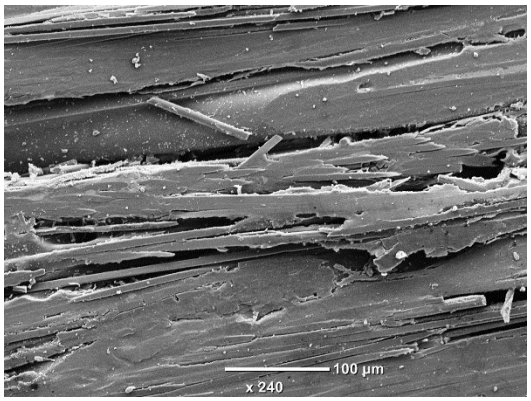

(d)

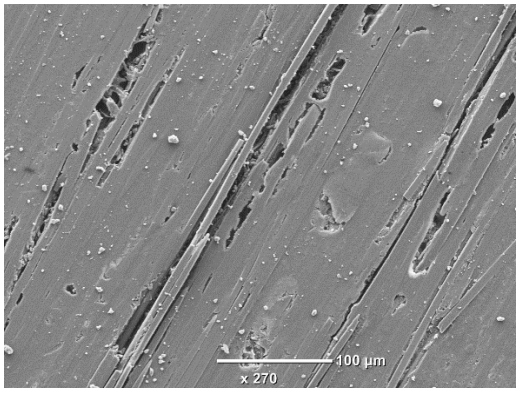

(e)

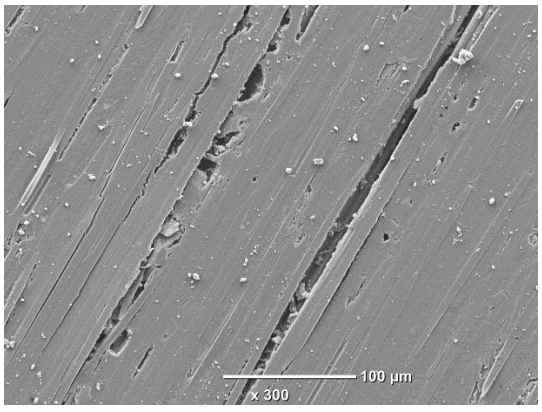

(f)

Figure 25. SEM of the worn surfaces of CCFC composites at different moisture. (a & b) Under dry condition; (c & d) Under 20 hours' water condition; (e & f) Under 240 hours' water condition

Chapter 6. Experimental and numerical investigation regarding scratch performance of 3D printed carbon fiber reinforced composites in moisture condition.

The wear performance of polymer composites was largely affected by the characteristic of sliding counterpart, as well as the fiber-polymer wear debris particles. To further understand how the wear debris affects wear behavior, an investigation on the microscopic origin of such debris was necessary. The effects of individual hard asperity on the wear of a polymer composite surface can be researched in micro-scratching experiment [51] A correlation could provide estimation of the similarity of macroscopic wear performance of a fiber-polymer composite material. The conical tip of a scratching experiment apparatus can be viewed as a hard asperity in the sliding counterpart of a tribosystem. Therefore, results from scratching experiment can be helpful for a deeper understanding the wear behavior of fiber-polymer composites [47].

Only a few studies reported on the fiber-polymer particle and damage mechanisms on a 3D printed fiber-polymer composite surfaces. This part focuses on applying the scratching test over a FDM 3D printed composite surface. Damage mechanism through the scratch tip was investigated. Particular attention was paid to the failure mode of the region around fiber-nylon boundary area.

6.1.1 Friction and wear properties

The lateral force and scratch depth were recorded for investigating the friction of 3D printed samples under a different load condition. Figure 26 presented the representative curves of lateral and normal force of SCFC and CCFC as a function of scratch distance with a load of 5 mN and 10 mN, respectively. It was noticed that scratch on SCFC surface presented a periodic variation in lateral force because of the presence of short

fibers. Scratching over the CCFC the friction was relatively stable as most of the contact area was between continuous fiber.

The frictional coefficient is calculated as the ratio of lateral force to normal load, $\mu = \frac{F_t}{F_n}$. F_t is lateral force while F_n is normal load. The friction coefficient was calculated through the steady state of scratch process for each specimen, shown in figure 27. Three identical experiments were averaged for each testing condition. The average frictional coefficient of SCFC was higher than CCFC under both 5mN and 10mN load condition. It inferred that scratching over SCFC surface the contact force was adhesion between indenters and nylon-fiber interface. The nylon of composite surface accumulated in front of the scratch tip, providing a rubbing effect, accompanying with nylon deformation mechanism during scratching. This increased the amount of adhesion force, and thus, rising the friction coefficient. By contrast, CCFC presented a small frictional coefficient. This could be attributed to the stiff continuous carbon fibers, enabling a small real contact area and low scratch depth. When indenter scratched over the stiff carbon fiber, a low lateral force was recorded.

It should be noticed that the friction coefficient scratched over the SCFC and CCFC both showed higher values under the load of 5mN. This was abnormal according to previous experiment [60]. One possible reason of this phenomenon could be the difference of deformation mechanism under different loads. In a light load condition as 5mN, composite surface experienced an elastic deformation, a rubber effect occurred, showing a relatively large amount of frictional coefficient. Under the 10mN load, indenter penetrated the surface deeply and then pushed forward. In this process, due to the filament voids because of the manufacturing process, and the porosities formation during printing, micro-cracks were easy to form in front of the indenter moving direction. This was followed by polymer prowling and detaching. This process would reduce the lateral force, and thus the frictional coefficient. To understand the involved

deformation and cracking mechanisms, the surface damage profiles were further examined by SEM.

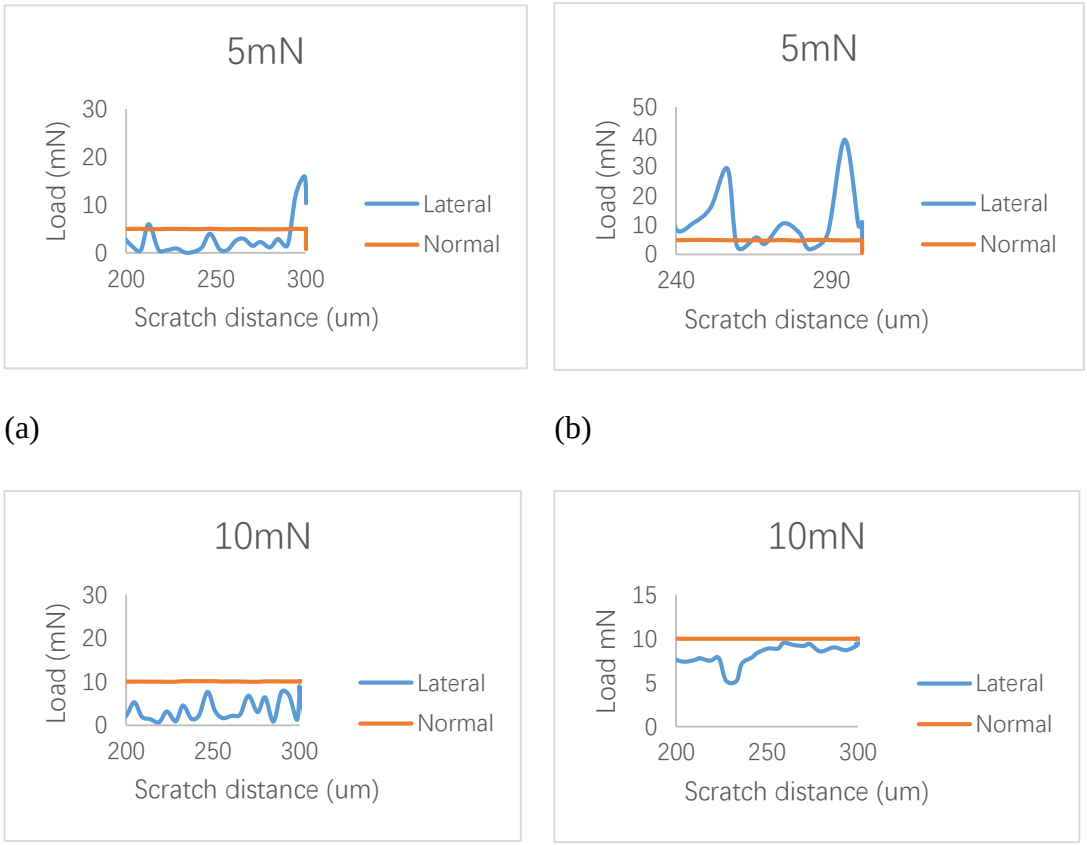

(a) (b)

(c) (d)

Figure 26. Representative evolution of normal & lateral force of CCFC and SCFC from 5-20mN. (a), (c), CCFC lateral force. (b), (d) SCFC lateral force

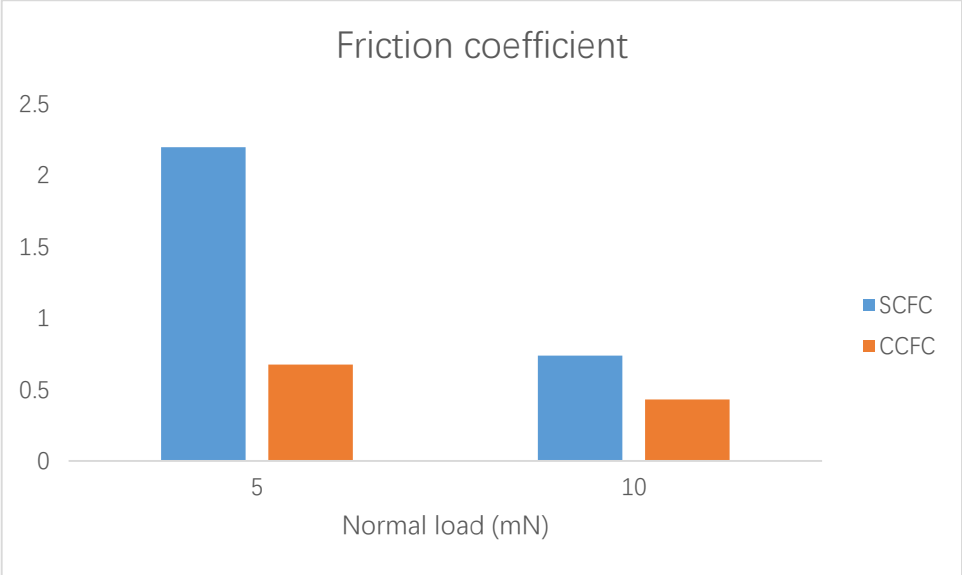

Figure 27. The average coefficient friction of SCFC and CCFC during scratching

6.1.2 Scratch damage analysis

To explore the scratch damage mechanism, SEM observation was necessary, as shown in figure 28 and 29. From figure 28, nylon presented a ploughed furrow when the scratch tip scratched across all different loadings. No severed carbon fiber debonding was noticed. This indicated that the formation of debris during scratching and tribology was mainly made of nylon. Under the load of 20 mN, instead of ploughing out the short carbon fiber, the scratch tip passed above the short fiber. This was equivalent to the asperity on the counterpart pushed downward the short fiber, making the short fiber sunk into the nylon before they were finally ploughed and removed from the composite surface. Nevertheless, as the normal load increased from 5mN to 10mN, the drop of friction coefficient could attribute to the separation and crack formation of polymer. As the nylon matrix was weak, friction coefficient decreased.

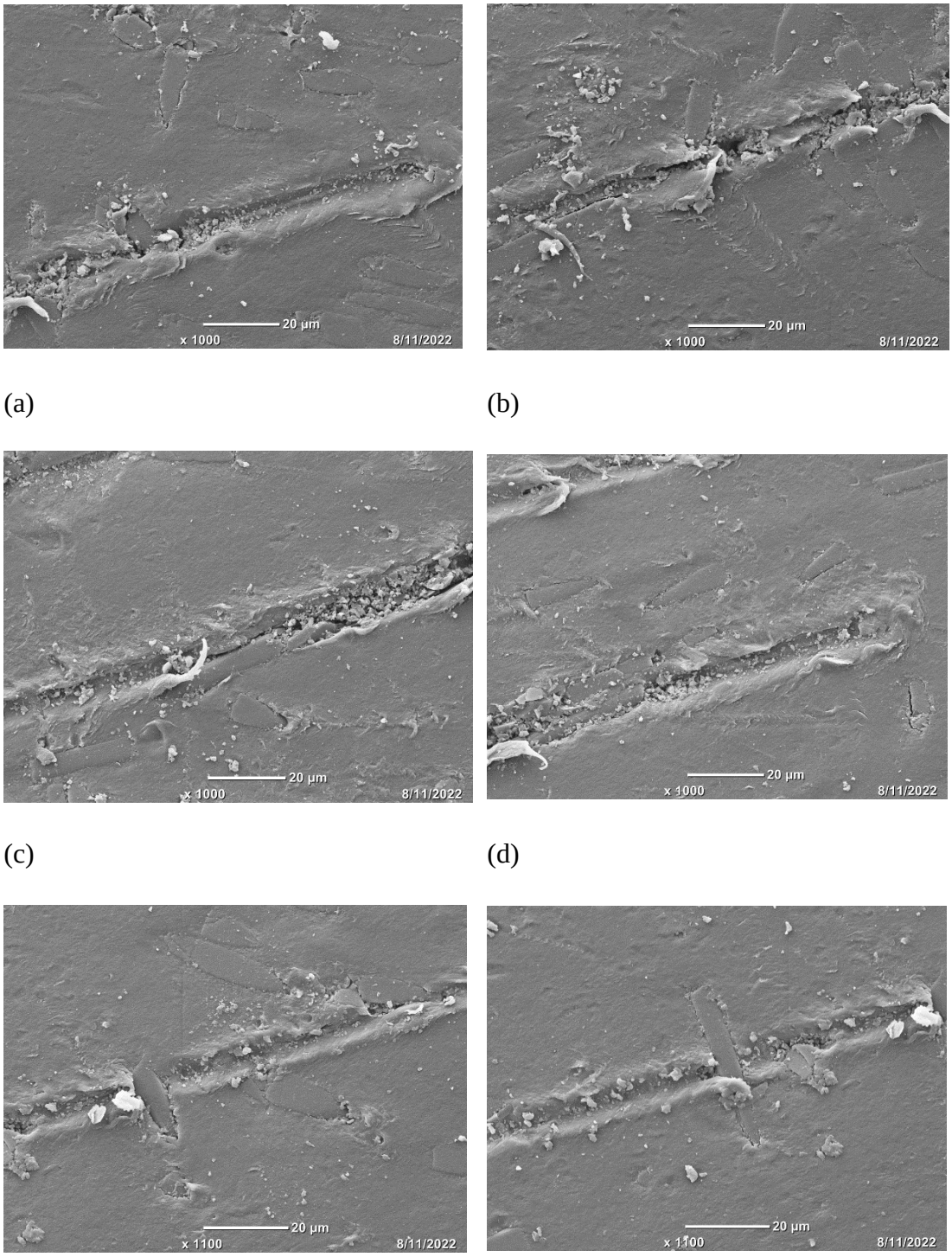

Figure 28. SEM micrographs of scratch grooves of SCFC under (a), (b) 5mN; (c), (d) 10mN, (e), (f) 20mN

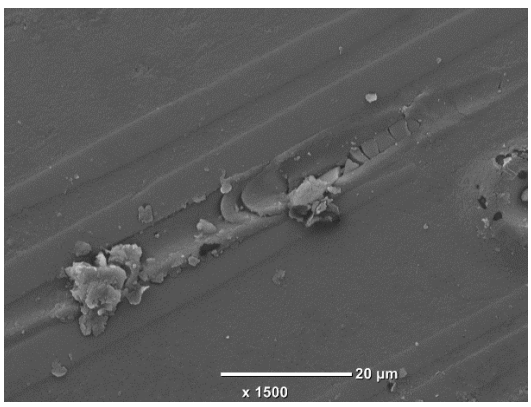

(a)

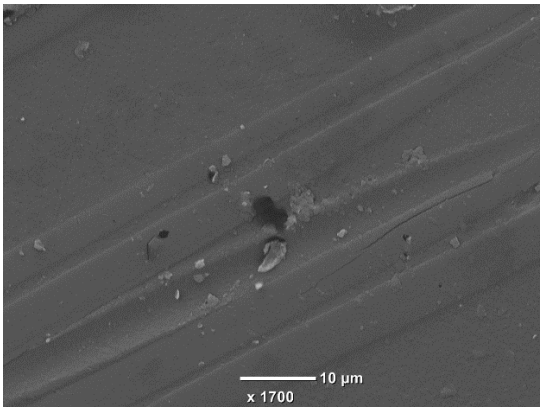

(b)

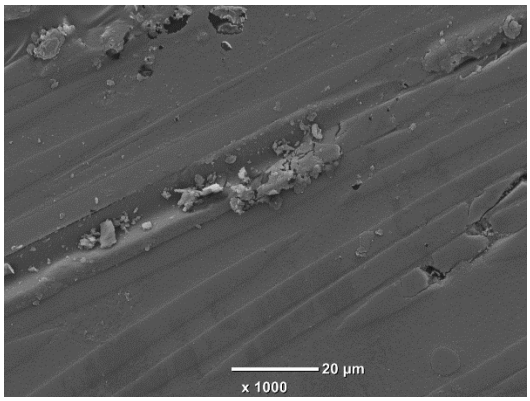

(c)

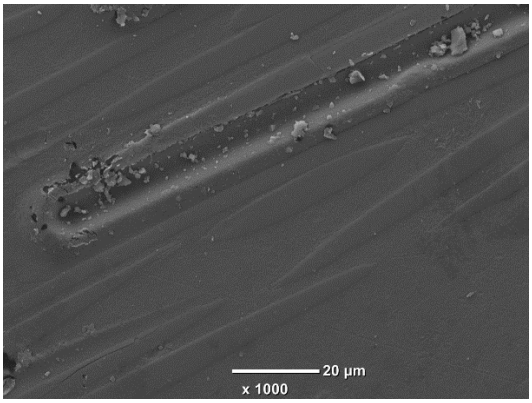

(d)

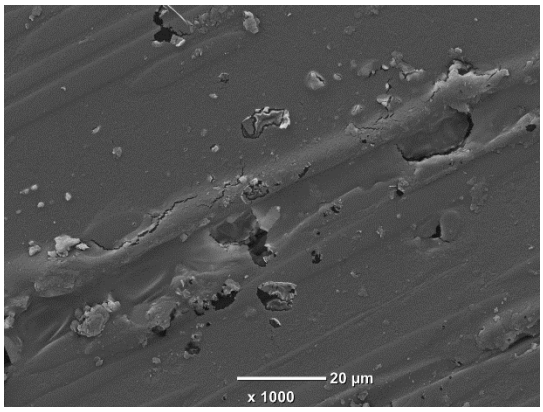

(e)

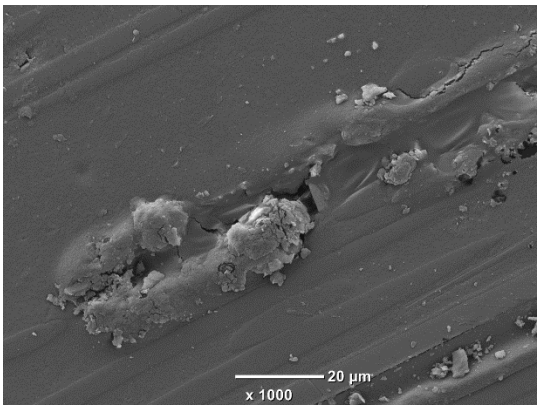

(f)

Figure 29. SEM micrographs of scratch grooves of CCFC under (a), (b) 5mN; (c), (d) 10mN, (e), (f) 20mN

The scratch deformation on CCFC surface was slightly different. When the normal load was relatively low, mild fiber-nylon cracking occurred when scratching in the fiber axis (figure 29a), suggesting a weak interfacial bonding. At the same time, some rippled formation waves were formed in the scratch direction, indicating that nylon debris stacked in front of the scratch tip, which was an adhesive wear phenomenon.

As the load increased to 10mN, fiber breakage was observed. Fiber fragments were located aside of the contact between tip and scratch groove. This indicated fiber fragments were pushed sideway when the tip scratched across, providing a better scratch resistance. Meanwhile, part of the fiber fragments remained in the composite surface, which also contributes to a better scratch performance. Therefore, friction coefficient of under 10mN load condition decreased. With a higher load up to 20mN, nylon matrix was damage severely. Nylon debris separated and spread across the scratch groove. Nylon debris was mostly removed from the surface. Fiber debris was also pushed heavily downward below the composite surface. This progress absorbed energy which could improve wear resistance. At the same time, due to the weak interfacial bonding strength of 3D printed filament, composites surface with voids and porosities below experienced nylon separation (figure 29e). The composites surface collapsed, leaving a hole or hollow section.

From the SEM images above, several scratch mechanisms could be concluded for 3D printed composites, such as slight abrasion, nylon ripple-like stacking, nylon debris formation, fiber-breakage, fiber removal, and scratch surface collapsing. As the load was low, slight abrasion and nylon ripple stacking were observed. With the increase in loads, we could observe fiber removal and the formation of nylon debris. Nylon matrix collapsing was also found. This means that the weak bonding strength of 3D printed continuous fiber filament deteriorated the scratch resistance.

6.2 Numerical investigation regarding scratch performance of 3D printed fiber-reinforced composites.

As it is discussed above, the damage mechanism of tribology experiment on the SCFC and CCFC surface under moisturized condition were mixed with polymer sliding grooves, polymer rupture, polymer debris fiber protruded, fiber removal and fiber breakage. These phenomena would be difficult to be observed and investigated directly through sliding wear tests. Instead, the numerical FEM modeling of a scratching test could provide hints to explain how these damage mechanisms were form.

The purpose of conducting the scratch numerical simulation was to acquire a deeper understanding into the mechanisms of tribology experiment of a fiber reinforced composites. The effects of additional fiber into the composites and interfacial bonding were investigated by analyzing the stress distribution during the scratch simulation.

6.2.1. Influence of different load on indenter for additive manufactured FRC

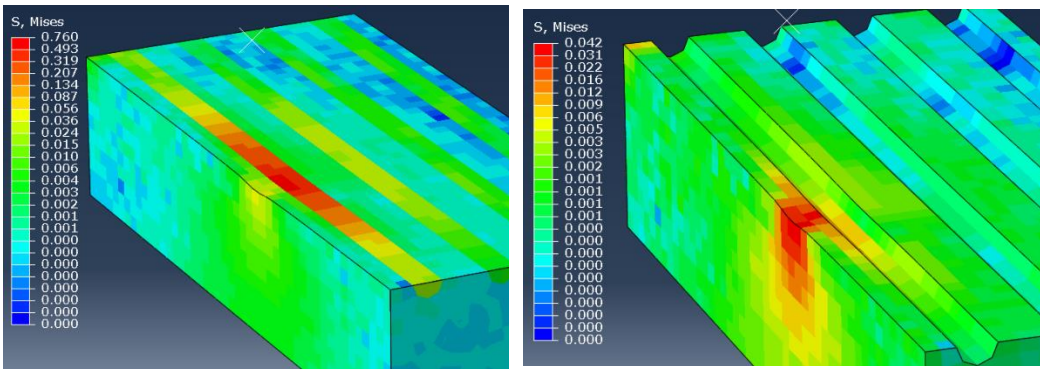

(a)

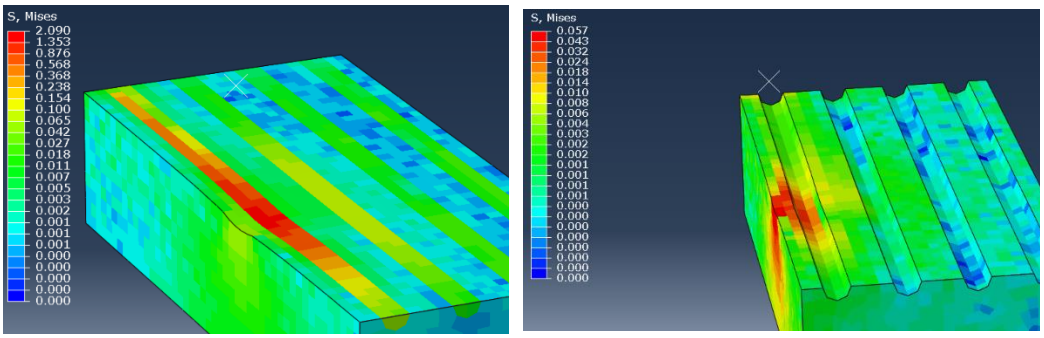

(b)

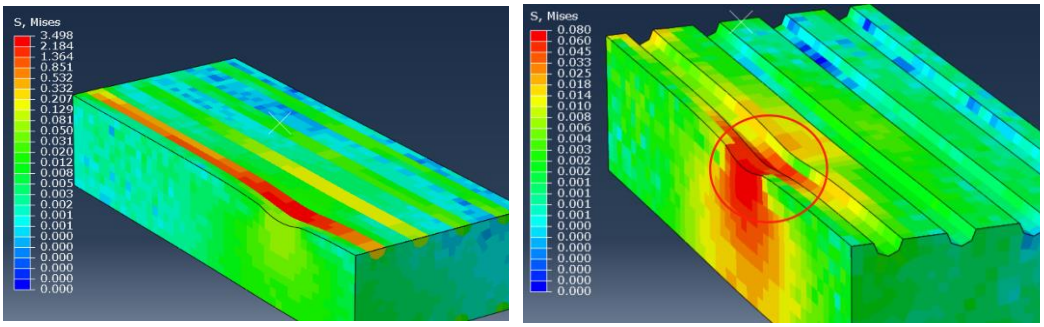

(c)

Figure 30. von Mises stress contour plot of fiber-polymer composites of 6.3% for a indenter load (a) 10mN, (b) 25mN, (c) 50mN, Right column of figure 31 was the contour plot of simulation results eliminating the fiber component.

It is known that the loading conditions on indenter affected the stress distribution and wear mechanism on FRC surface. Figure 30 presents von Mises stress of a 6.2% volume fraction fiber-polymer composites of an indenter force range from 5mN to 50mN. All other parameters were set to be constant. When the load is relatively small, fibers near to the scratch indenter took most of the load, no obvious stress concentration could be found in figure 31a. Compared with a low load condition, indenter under a high load condition led to the stress extended through the fiber longitudinal direction toward both ends. The peak stress was observed right beneath the indenter tip. This agreed with the experiment results that the wear behavior of heavy load usually led to fiber breakage because stress on fiber below the scratch tip exceeded its critical strength.

The high level stresses in the polymer component could be observed in the fiber-polymer interfacial regions in the bottom part of fiber, circled in figure 30c. Such phenomenon was also observed by Goda et al [39]. This indicated that cracks were form easily in this area due to stress concentration. Debonding was likely to occur. Both polymer and fiber did not yield to its maximum tensile strength in FE simulation. But in reality, cracks and debonding had already observed. In this work, FE simulation only considered the elastic situation for stress analysis. Also, the formation of voids and

porosities in additively manufactured specimens led to a weaker material strength. Stress transferred longitudinally along the fiber to both ends, and stress concentration was not observed on polymer. The stress difference of fiber-polymer could lead to fiber debonding.

The stress distribution presented in figure 30 supported the proposed damage mechanism for the scratch experiment. This indicated the FEM modeling in this thesis was valid. The model can be used for further numerical analysis. In the rest of this chapter, different scratch parameters on affecting the scratch performance. Scratching parameters can be classified in two categories. One was composite parameters, including the volume fraction of fiber and polymer strength under a moisturized condition. Another one was scratch tip parameters which were load on tip and radius of tip.

The stress distribution can be well explained and correlated to the damage mechanisms in the SEM presenting previously. In this case, the FEM modeling in this thesis was verified and valid. Other scratching parameters can be adjusted for further stress distribution analysis. By this way, it could comprehensively study the factors that affecting the scratch performance.

6.2.2. Influence of different fiber volume fraction for additive manufactured fiber reinforce composites (FRC)

As reported in tribology experiment chapter, different fiber volume fraction posted a significant change in wear mechanism. Therefore, the effect of fiber volume fraction as a parameter was particularly studied. Figure 31 presented the von Mises stress distribution under the same applied load with different fiber content in FRC. The 10mN load was constant at all the time. As the fiber volume fraction increased, the von Mises stress of fiber increased, while the stress on polymer decreased. This could attribute to the stress transformation, from polymer to the fiber. Each unit length of fiber took a

larger amount of load than polymer. Looking at the stress distribution, stress was transferred in the fiber longitudinal direction. A low fiber volume fraction, i.e, 3%, von Mises stress on polymer concentrated around the indenter. Accordingly, polymer broke into small pieces due to high stress concentration, leaving fiber to be extruded from the surface. By contrast, when the fiber content was high, stress on polymer spread along the scratch direction relatively uniform. Polymer was less likely to be breakage. Instead, fiber breakage occurred due to the high stress on it. Also, a great difference of stress between polymer and fiber caused the stress mismatch, which could lead to fiber debonding.

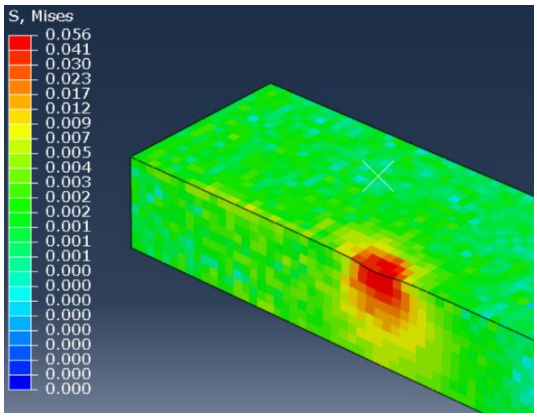

(a)

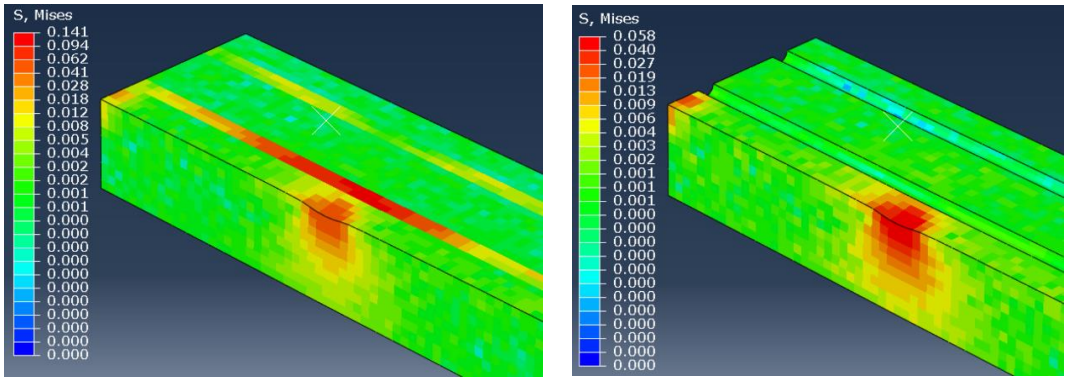

(b)

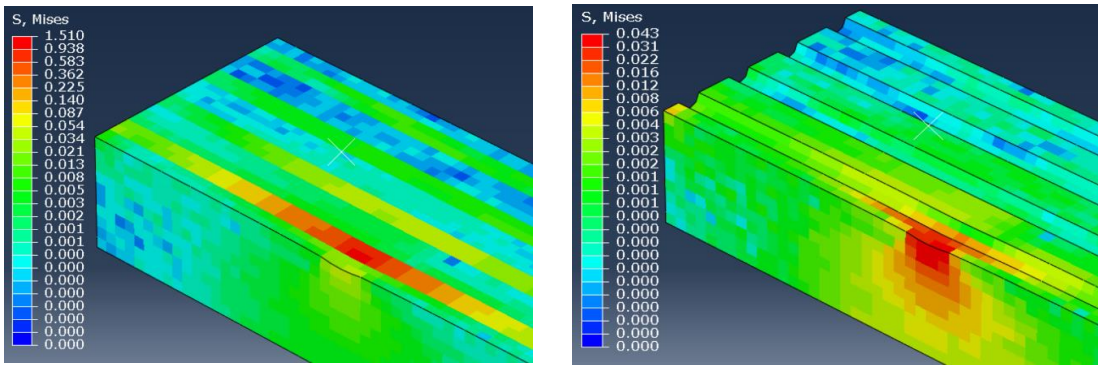

(c)

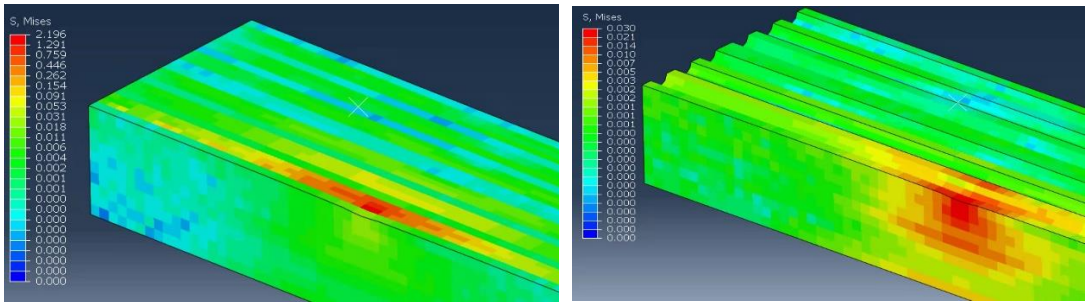

(d)

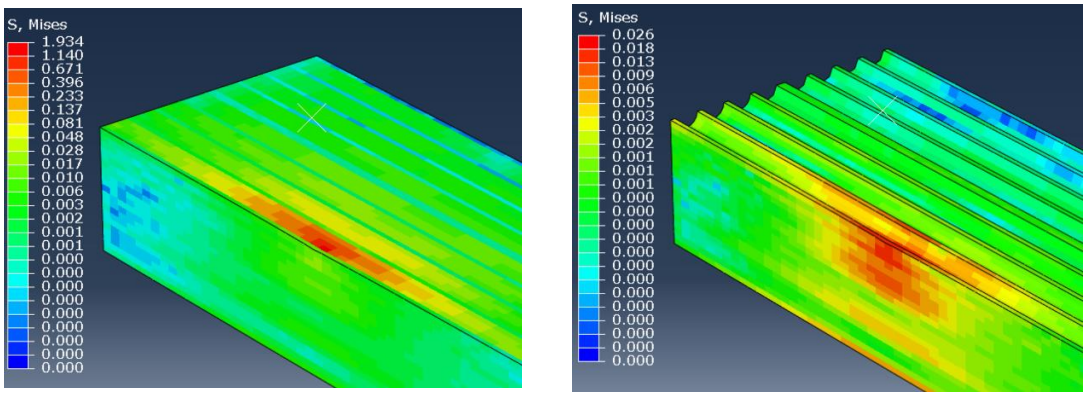

(e)

Figure 31. von Mises stress contour plot of fiber-polymer composites at 10mN for (a) neat polymer (b) 3.1% volume fraction (c) 6% volume fraction (d) 18% volume fraction (e) 38% volume fraction; left hand side images show contour plot for composites, right side images show contour plot for polymer matrix.

6.2.3. Influence of different indenter radius for FRC

In tribology experiment, each asperity in the steel counterpart had different sharpness. It means the radius of asperities was different, which produces a different wear mechanism for each asperity sliding across the composite surface. To further understand how the difference in asperity radius affects the wear and scratch mechanism over a fiber-polymer composite surface, a simulation working on investigating the effect of indenter radius would be helpful.

Indenter radius scratching over the FRC surface in FEM posted differences in stress distribution. Figures 32-34 show the von Mises stress distribution with an indenter radius of 30um, 50um and 75um, respectively under the load condition 10mN and 50mN. It is clear that the von Mises stress on fiber increased from 2GPa to 2.7GPa, as the radius of scratch indenter increased from 30um to 75um under a load condition of 10mN. At the same time, stress on the polymer remained stable. It can attribute by the increase contact area between indenter and fiber. Each unit length of fiber took more load, providing support for the composites surface of downward bending. In a small load condition (10mN), a large contact area could provide protection from the polymer breakage. In reality, the damage mechanisms in tribology were more likely to be fiber breakage and fiber bending. This was because the stress was mainly concentrated in fiber. The stress mismatch between fiber and polymer caused debonding. On the other hand, fiber underwent plastic deformation under a high load condition (for example: 50mN). This could be related to fiber bending in tribology damage mechanism, if fiber has passed its yielding strength but polymer beside the fiber was still in elastic deformation.

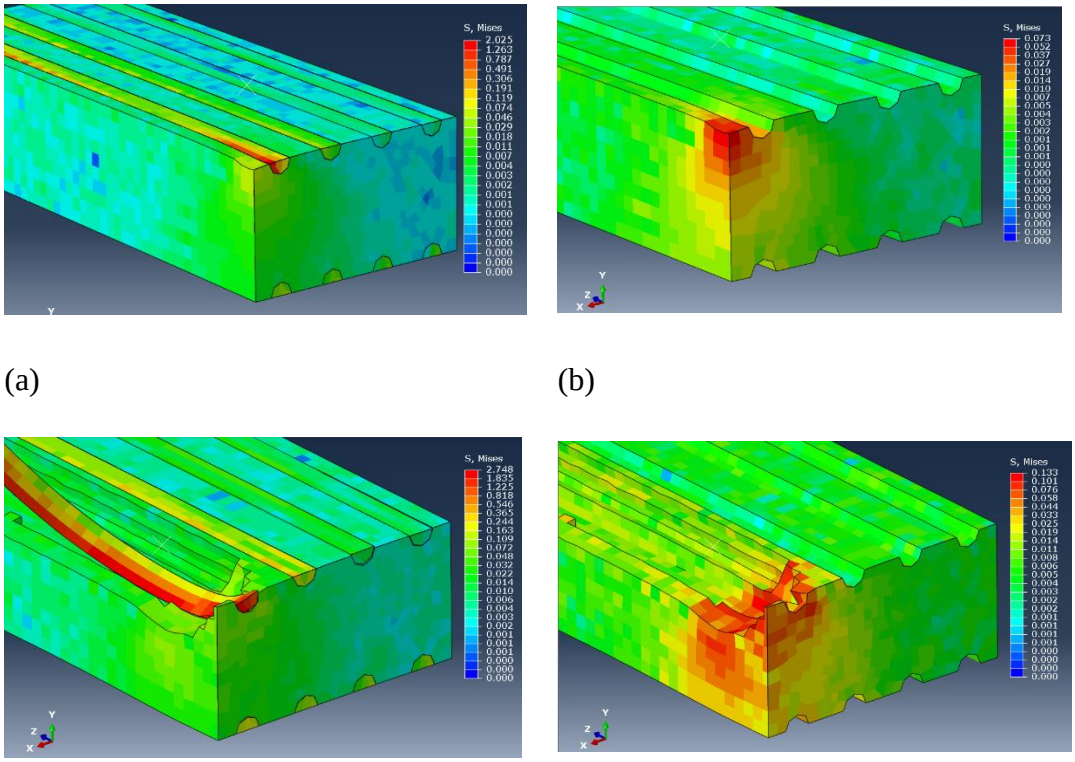

(a) (b)

(c) (d)

Figure 32. von Mises stress distribution under an indenter radius of 30um under a load condition of 10mN (a, b) and 50mN (c, d).

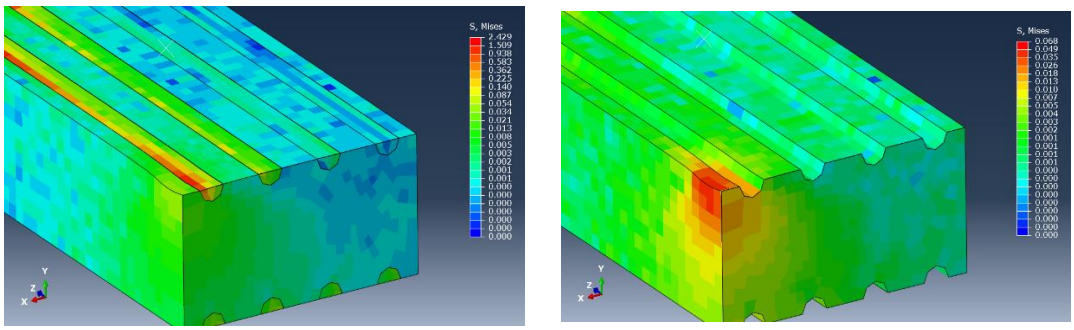

(a) (b)

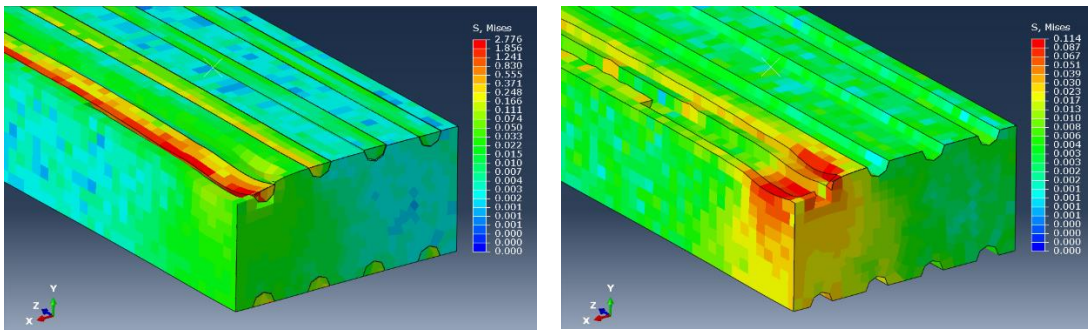

(c) (d)

Figure 33. von Mises stress distribution under an indenter radius of 50um under a load condition of 10mN and 50mN.

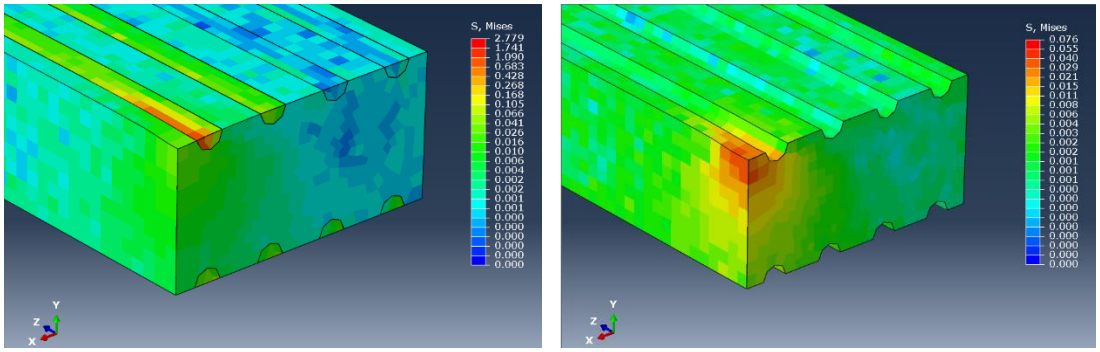

(a) (b)

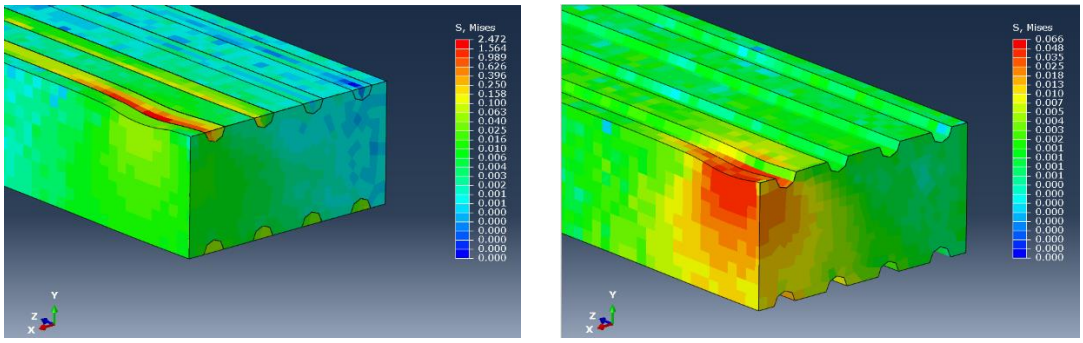

(c) (d)

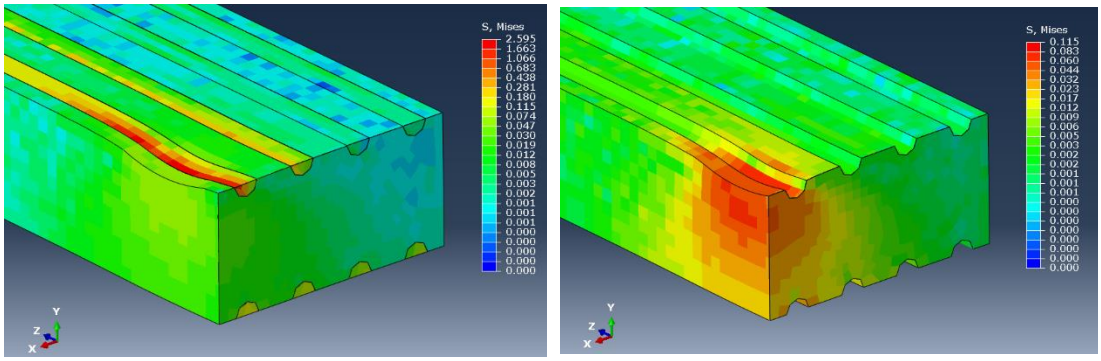

(e) (f)

Figure 34. von Mises stress distribution under an indenter radius of 75um under a load condition of 10mN and 50mN.

In a high load condition, there was no significant change of the von Mises stress distribution for a large indenter scratching over the composite surface, as the fiber was giving enough protection against a blunt indenter. Load was uniformly transferred from polymer to the corresponding fiber. Therefore, before the polymer underwent plastic deformation, fiber could withstand a higher load. However, a small radius indenter (30um) posted severed damage to the polymer part, shown in figure 32c. It was beyond elastic and plastic deformation. Instead, polymer was completely ripped off from the surface. Corresponding to the wear surface tribology experiment, this could be represented by the formation of small grooves and polymer rupture in a tribology wear surface. Polymer was scooped out from the composite surface, while leaving the fiber on the surface. For the fiber damage mechanism, fiber protruded could be observed at first because of the critical damage of polymer. Eventually, fiber removal could occur.

It should be also noticed that the failure modes between blunt indenter and sharp indenter were different. Under the scratch of a sharp indenter (30um radius), polymer was breakage initially because the indenter was digging up the polymer. Without the support of polymer, fiber protruded and removed easily, showing a weak scratching and wearing performance. Fiber embedded in FRC did not maximize their duty to increase the scratch or tribology performance.

Under the scratch of a moderate sharp indenter (50um radius), it provided a clear view on how the polymer failed. The polymer cracking was initiated from the bottom part of the fiber, shown in figure 33c. Once polymer cracking exceeded the critical strength, polymer failed and fiber on top was pushed downward, probably without fiber breakage. The fiber breakage occurred if the loads kept increasing, or sliding repeatedly and eventually, polymer and fiber were removed simultaneously from the surface. In this progress, cracking between fiber and polymer could be observed. Fiber breakage and removal could be found at the same time.

When scratching by a blunt indenter, (75um radius), fiber breakage could be observed the most as load was most likely to be transferred from polymer to fiber, to protect the matrix phase. It was followed by the debonding due to the stress mismatch between fiber and polymer, while polymer cracking would be less likely to observe.

To further investigate the stress evolution, the maximum principal stress contours were given to illustrate the tensile or compressive stress for every component. The results are presented in figure 35 and 36. We eyed on stress states in the contact region when the indenter was scratching over. The maximum principal stress contours under a scratch radius of 30um were not presented as fiber and polymer were completely destroyed. Looking at figure 35, the polymer contour plots indicated that if no plastic deformation occurred, polymer under the indenter went through compressive stress while polymer behind the indenter experienced tensile stress. This could imply that polymer cracks were in the tensile region and polymer debris was form in the underneath the indenter due to the compressive stress. At figure 35a, when plastic deformation and failure were initialized, polymer in front of the scratch direction experienced a tensile stress. It was because polymer behind the might fail already and thus the composite surface was lower. Polymer in front of the scratch direction was bended downward and showed tensile stress.

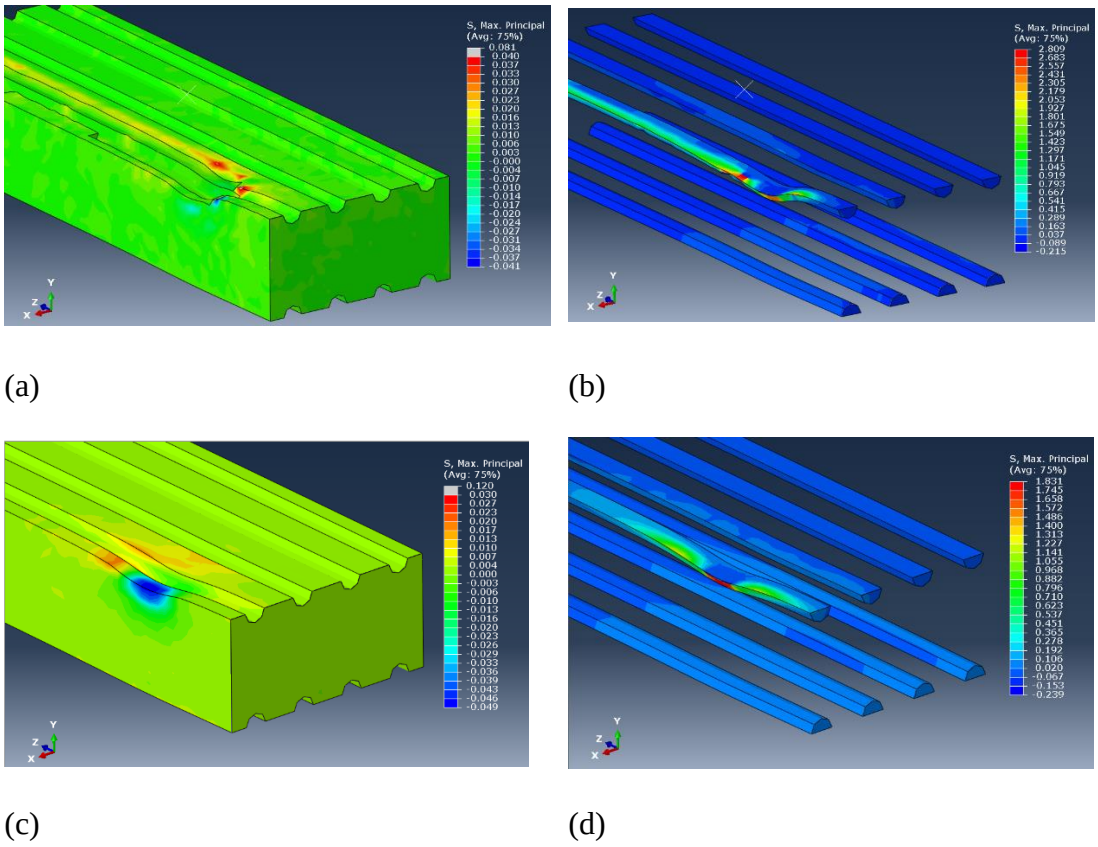

Figure 35. Load under 50mn for each component with different indenter radius. (a) & (b) 50um radius. (c) & (d) 75um radius.

The fiber part of both indenter radiuses presented a similar maximum principal stress distribution, with the exception that a higher tensile stress in front and behind the scratch indenter was observed for a high load condition. High tensile stress was found along the scratch direction behind or in front of the indenter, with the exception of fiber that was located right underneath the scratch tip. Therefore, cracking was likely to occur in the former position. On the other hand, debonding was easy to occur for the fiber underneath the scratch tip because there was a great stress difference between fiber and polymer. In reality of both scratch and tribology experiment, as the weak bonding between fiber and polymer was evitable for a FDM 3D printed composites, debonding was more obvious, fiber was easy to detach.

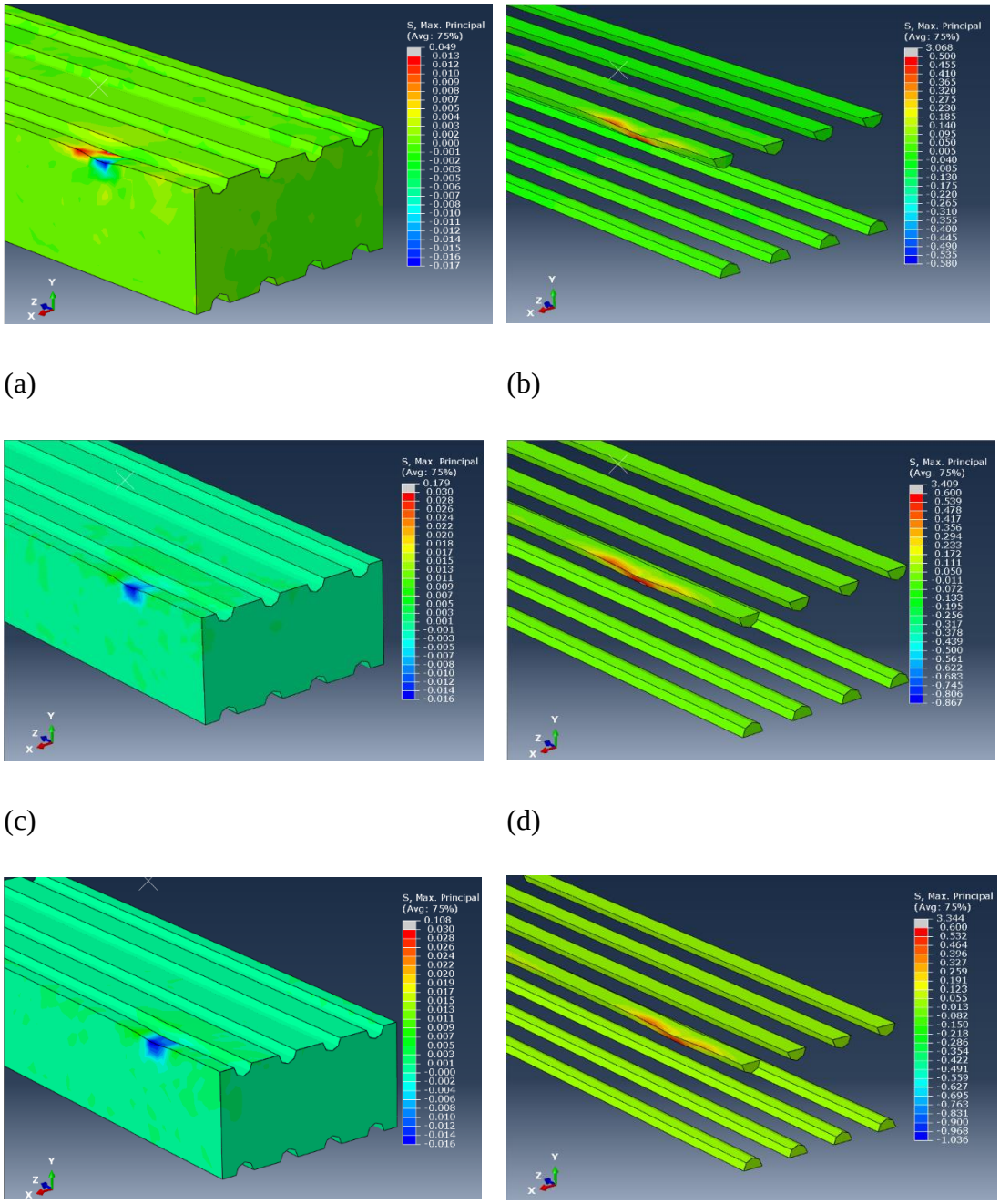

Figure 36. Load under 10mN for each component with different indenter radius. (a) & (b) 30um radius. (c) & (d) 50um radius. (e) & (f) 75um radius.

Figure 36 indicates the scratch simulation under a light load situation. Under a 10mN load, fiber-polymer composites surface went through plastic deformation, especially

for a sharp indenter, shown in figure 36a. This provided a convenient way to carry out stress distribution analysis. Looking at the polymer component in figure 36a, c & e. A sharp indenter resulted in great tensile stress on the polymer, while only compressive stress was observed under a 50 and 75um radius indenter. If we related this with the scratch and tribology test, a conclusion can be drawn as that a sharp indenter posted significant damage to the polymer part of the composite surface. It could observe deep grooves and a large amount of polymer debris during sliding. On the other hand, a blunt indenter would be difficult to destroy the polymer component alone. Polymer cracking and debris were hard to observe. Comparing with the maximum principal stress on fiber component, stress area around the tip scratched by a sharp indenter was much smaller than a blunt tip, shown in figure 36d & f. However, the peak value of maximum principal stress among three indenter radius was similar. This can only draw up a conclusion that fiber sliding & scratching against a sharp tip provided little help on protecting polymer. It would be difficult to deduce the wear and scratch damage mechanism based on fiber stress distribution.

6.2.4. An attempt to simulate the moisturized condition of FRC using FEM.

There were a lot of factors contributing to the deterioration of FRC under a water absorb condition. In previous research [1], some parameters were quantitatively measured. In the FEM modeling, the dominated quantitative parameters were young's modulus and tensile strength. The young's modulus and tensile strength of polymer would reduce by 50% at a moisture level of 4wt%. Therefore, to make it consistent in my model, I reduced the young's modulus and tensile strength of polymer by 50% to in the FEM modeling. The young's modulus and yield stress were set to be 200MPa and 50MPa, respectively. The mechanical property of fiber remained the same as moisture posted little effects on fiber's property.

To make it simple and easy to visualize, I selected the FEM model of an indenter radius 50um and the fiber volume fraction of 6.2% of simulation. The load was selected 5mN, 10mN and 25mN. Figure 37 presented the von Mises stress of the composite surface of

the load from 5mn to 25mN under a moisturized condition. Figure 38 presented the von Mises stress of the polymer component only under a moisturized condition. Under a light load condition, von Mises stress on fiber in water condition was greater than that in dry condition. Stress was extended toward both side the fiber. It can be attributed that polymer took less amount of load and thus fiber must take more load.

Compared with dry condition, polymer reached the yield stress sooner, at 50MPa. Figure 38b, d & f showed more severed plastic deformation occurred in water condition composites. The von Mises stress on polymer under a high (50mN) load condition spread deep beneath the sample. In reality of a 3D printed samples, this might result in polymer failure because 3D printed composites involved a lot of defects, voids and porosities. At the same time, the stress distribution from FEM simulation could be correlated to tribology experiment damage mechanism. In a tribology experiment, large pieces of polymer with fiber were removed. Grooves, polymer debris and other plastic deformation on the surface could be found. Debonding was initialized inside the polymer due to the weaker mechanical property of polymer after absorbing water.

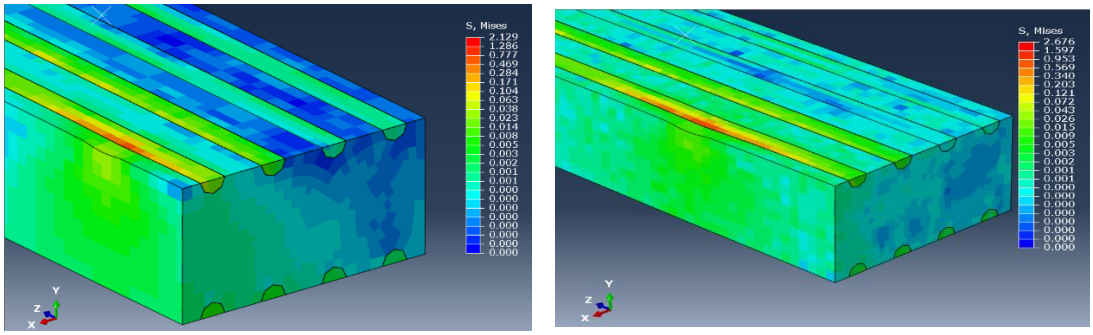

(a) (b)

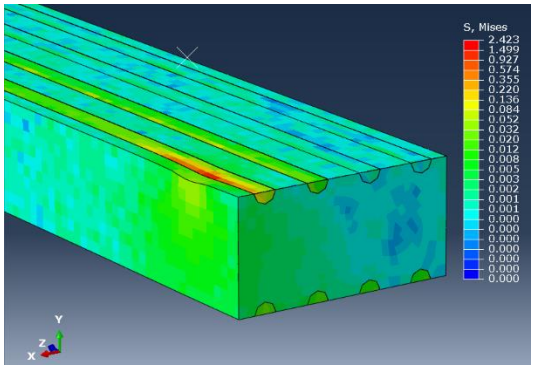

(c)

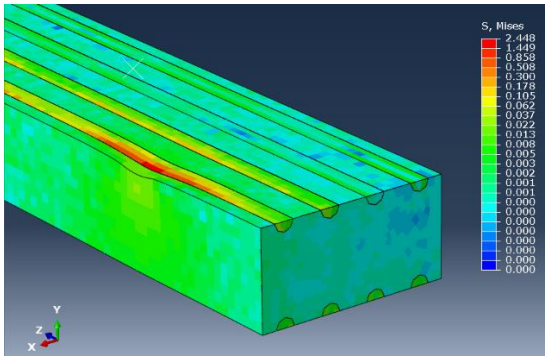

(d)

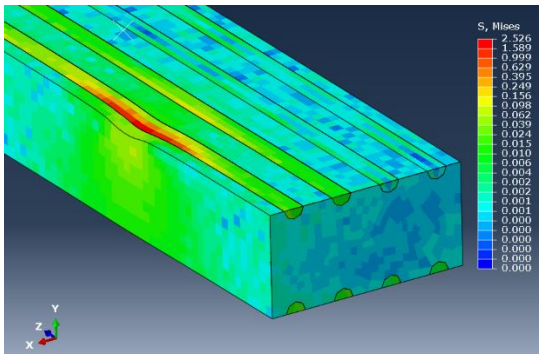

(e)

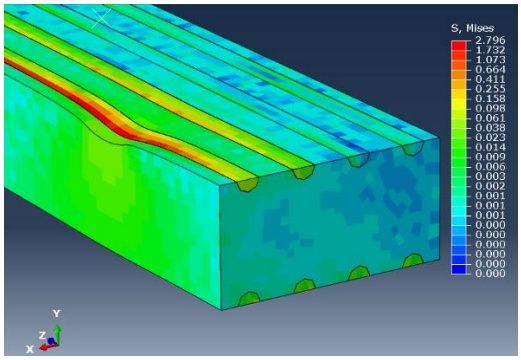

(f)

Figure 37. Von Mises stress on composite surface with different loads. Left column is the stress in a dry condition and the right column is the stress of a moisturized composite surface. (a) & (b) 5mN load. (c) & (d) 10mN load. (e) & (f) 25mN load.

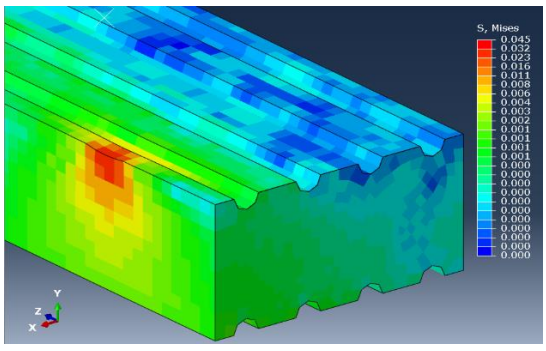

(a)

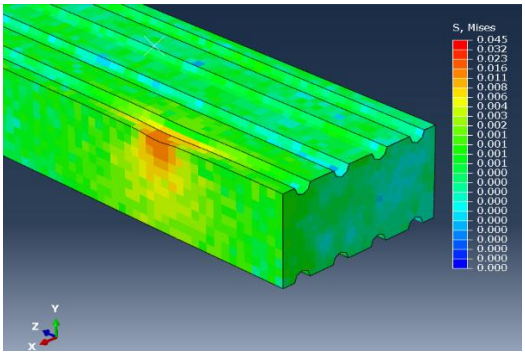

(b)

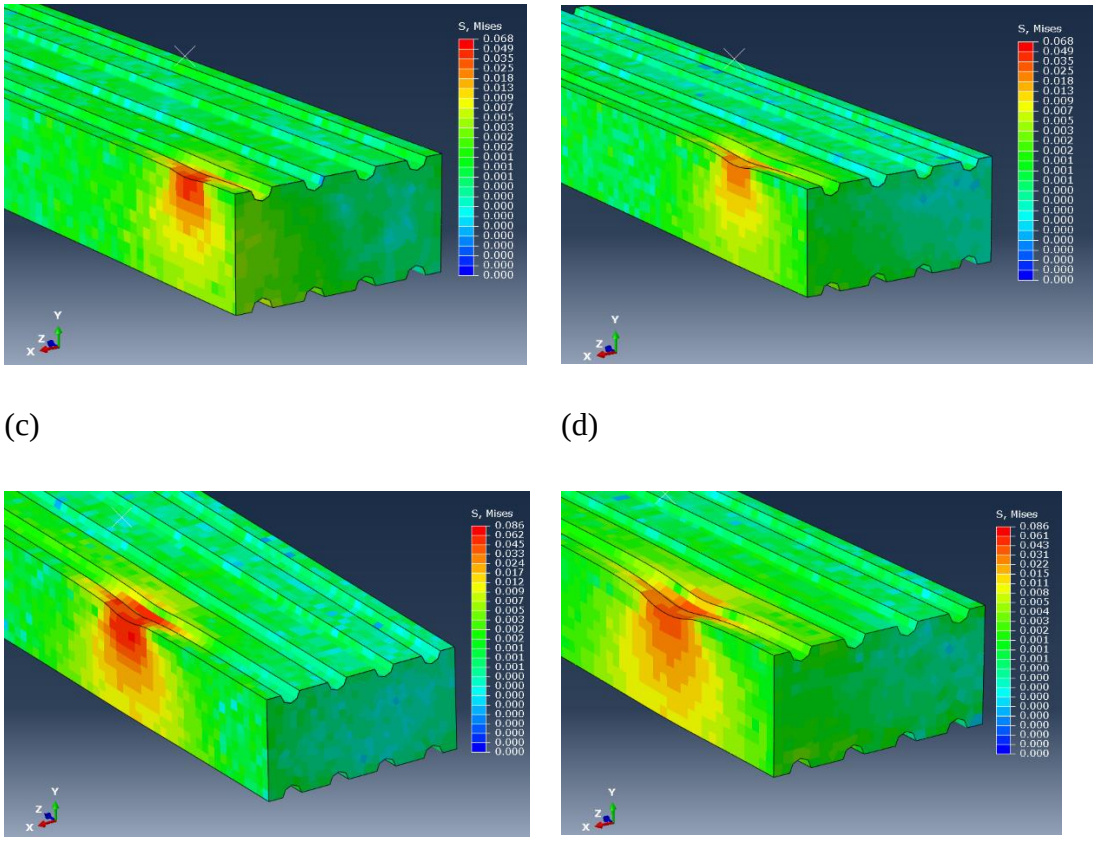

(c) (d)

(e) (f)

Figure 38. Von Mises stress on polymer component with different loads. Left column is the stress in a dry condition and the right column is the stress of a moisturized composite surface. (a) & (b) 5mN load. (c) & (d) 10mN load. (e) & (f) 25mN load.

The maximum tensile stress in front and behind the scratch tip could be used to analyze the crack formation during the scratch process. Figure 39 showed the magnitude and direction of maximum principal stress contour plot of fiber component at 6.3% volume fraction with different load under both dry and water absorbed condition. Tensile stress on fiber did not show a noticeable difference if composites were in water condition under a low and moderate load condition. Both tensile and compressive stress did not show a significant change. It was because although polymer was soften after immersing in water, it could still resist a low scratch and tribology environment. Therefore, it showed no difference in stress distribution. A high load condition eventually indicated that a greater region of tensile stress occurred in front and behind the scratch tip, causing

a fiber cracking. A slightly high compressive stress was also found on fiber underneath the scratch indenter.

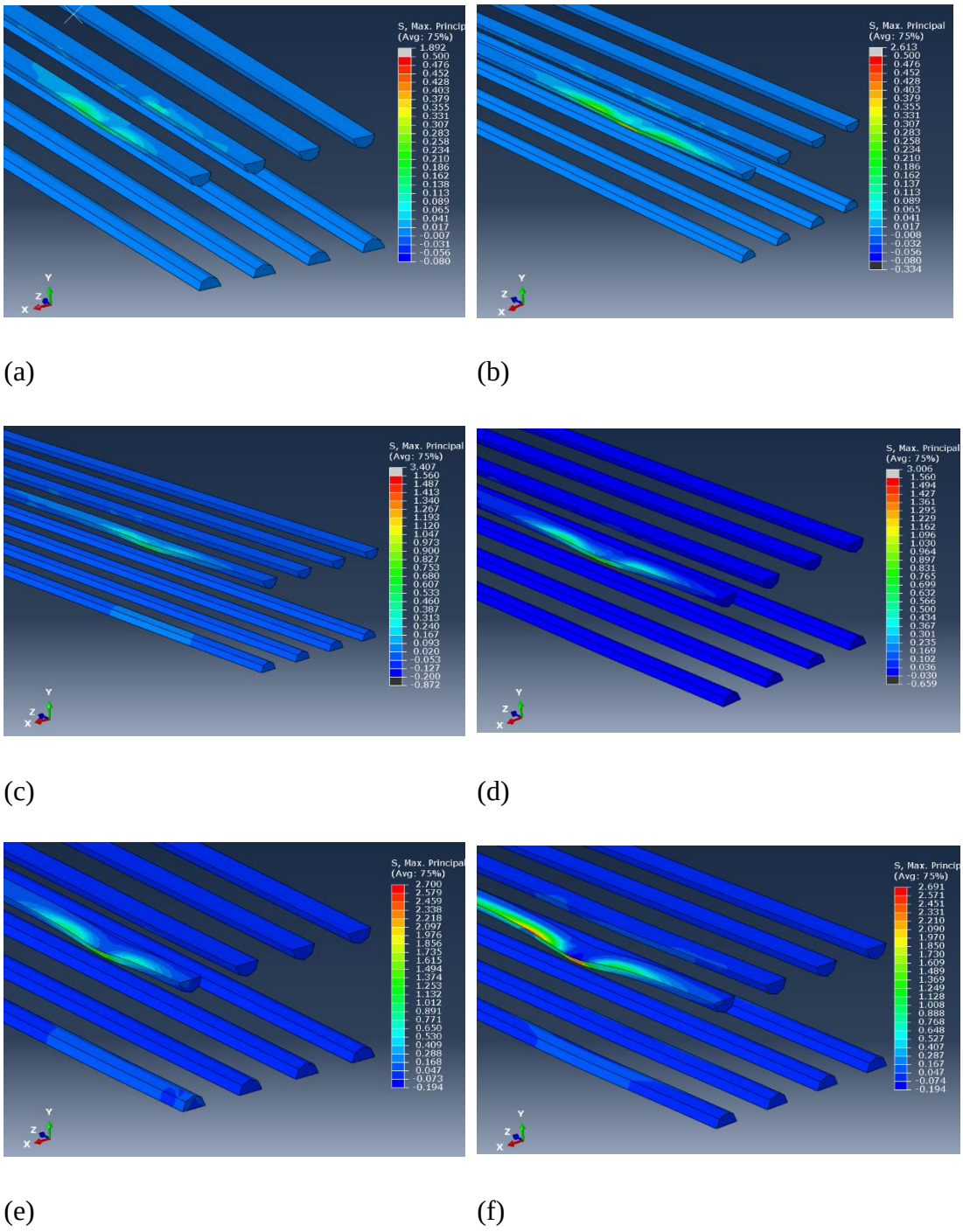

(a) (b)

(c) (d)

(e) (f)

Figure 39. Maximum principal stress on fiber with different loads. Left column is the stress in a dry condition and the right column is the stress of a moisturized composite surface. (a) & (b) 5mN load. (c) & (d) 10mN load. (e) & (f) 25mN load.

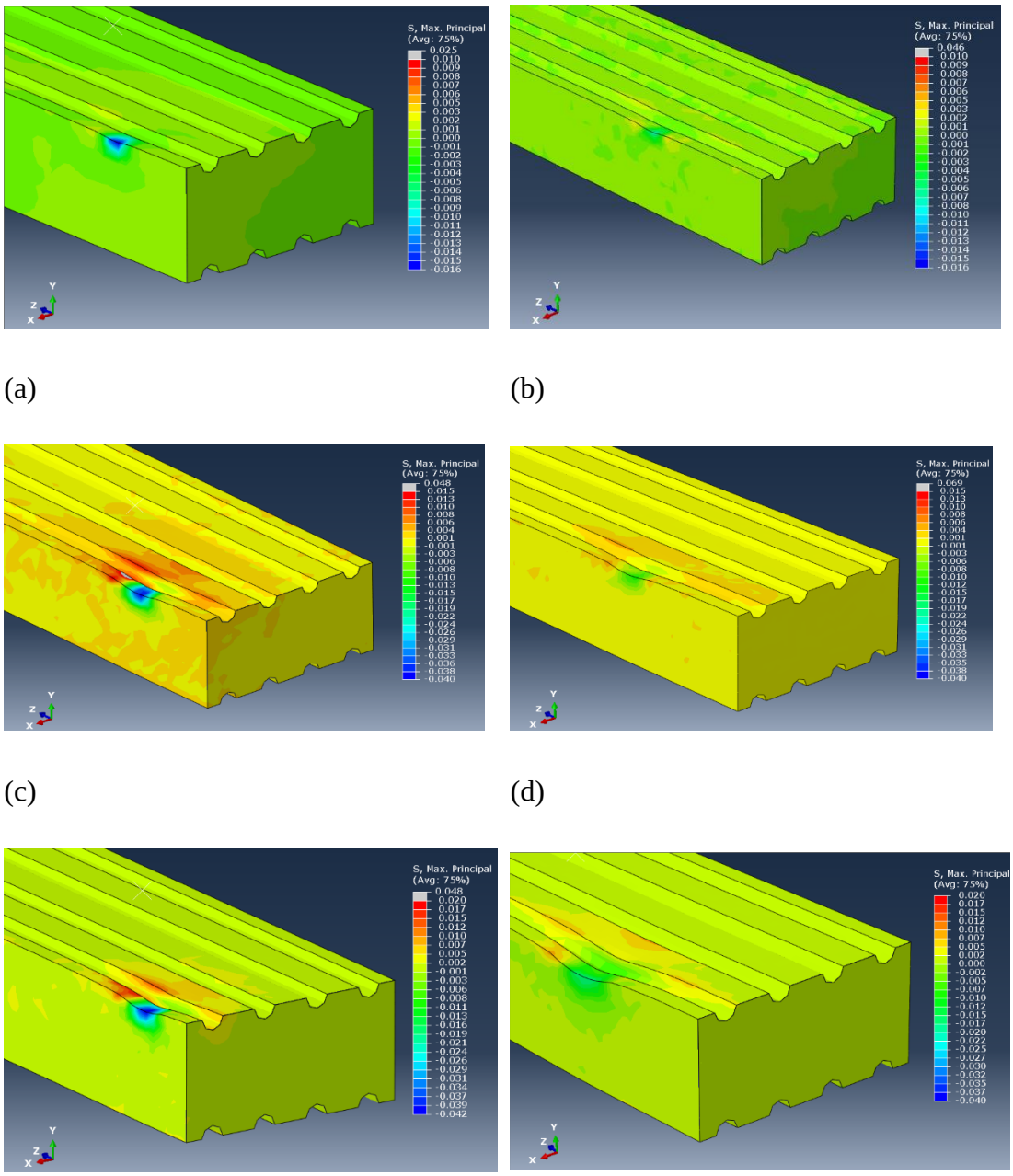

Figure 40. Maximum principal stress on polymer component with different loads. Left column is the stress in a dry condition and the right column is the stress of a moisturized composite surface. (a) & (b) 5mN load. (c) & (d) 10mN load. (e) & (f) 25mN load.

Figure 40 illustrated the maximum principal stress distribution on polymer simulating a moisturized condition. Polymer scratched under dry condition showed a higher maximum principal tensile and compressive stress than that in moisturized situation. A softened polymer was not able to take high amount of loads. A large principal compressive stress was found under high load. In reality as polymer was compressed extremely hard, the formation of debris occurred due to high shear stress components. It should also notice that stress was concentrated on polymer under dry condition while it dispersed if it absorbed water under a 25mN load condition. This stress distribution characteristic provided useful hints and visualization for analyzing the wear and scratch behavior in tribology and scratch test.

In figure 40c & e, the dry polymer showed a small deformation but presenting high stress concentration. It was tested that polymer property was brittle under dry condition. These can conclude polymer cracking dominant the damage mechanism under dry condition. On the other hand, the polymer property became ductile and soft, with low yield strength when immersed in water. A dispersed stress distribution around the indenter with a low principal stress value was found. Polymer experienced the severe deformation which could be found in figure 40f. However, fiber property remained unchanged after the water immersion. It still presented the brittle and strong mechanical properties. The huge difference of mechanical properties between fiber and moisturized polymer caused the ‘slipping’ between fiber and polymer during tribology test, and then debonding occur.

Chapter 7. Conclusion

In this thesis, the mechanical and tribological properties of short and continuous carbon fiber composites (SCFC and CCFC) fabricated by Mark Two 3D printer were investigated under different moisture levels. The scratch tests were conducted to study the composite surface damage mechanism. A FE model was also established to reveal the stress distribution in composites during the scratching test, in order to further understand underlying mechanics in CFCs under different loading conditions.

The results showed that the tensile strength of all the fabricated specimens, namely neat nylon, SCFC and CCFC was decreased under a moisturized condition. In particular, different damage mechanisms between SCFC and CCFC were observed. For a moisturized SCFC, the tensile strength, damage mechanisms and sample failure characteristics were greatly affected by the interfacial properties between fiber and matrix. As a result, it showed a more severe damage and a greater drop of tensile strength with water absorption. During the tensile tests, short carbon fibers were easily to be pulled out. On the other hand, the tensile properties of CCFC were mostly dependent on fibers, showing a less sensitivity to moisture absorption.

The tribology experiments indicated that SCFC specimens presented an increased friction coefficient and specific wear rate under a moisturized situation, while the wear rate and friction coefficient for CCFC's were both decreased. For SCFC, the increased friction coefficient of the moisturized SCFC can be explained by more severe plastic and viscoelastic deformation in matrix, which also contributes to a severed worn surface. Large sections of polymer debris were peeling off from the worn surface. Fiber removal was observed. On the other hand, wear performance of CCFC improved under a moisturized condition. This was mainly because a high volume fraction of continuous fiber governs the mechanical performance of the composite material, which is little affected by water absorption in matrix. Each unit fiber length enabled to take a large

amount of the load, despite the strength reduction of nylon matrix. Moisture trapped inside the hollow sections, voids and porosities of nylon-fiber interfacial regions provided a lubricating effect during sliding.

The effects of fiber composite and scratch parameters, i.e. fiber volume fraction, scratch indenter radius and polymer strength under moisture condition, were also investigated using numerical method. The following conclusions can be drawn:

- A high volume fraction of fiber can transfer more load from polymer to fiber. Stress on polymer decreased while on fiber increased. Polymer debris was less likely to form but fiber breakage may occur.
- A small indenter radius scratched over the composites surface caused a severed damage to the polymer part due to the stress concentration. Fiber protruded initially due to the critical damage of polymer, and eventually, fiber removal occurred easily. On the other hand, scratch by a large indenter radius was likely to cause fiber breakage and fiber-polymer debonding due to the stress mismatch.
- Polymer turned to be ductile and have low yield strength under a moisture condition. This resulted in the stress spread beneath the moisturized composites sample. In a real 3D printed fiber reinforced composites, with the addition of voids and porosities, polymer was more likely to fail. Scratching posted more plastic deformation and cracking to the polymer component.

Reference:

1. N. Jia and Howard A. F. Effects of Moisture Conditioning Methods on Mechanical Properties of Injection Molded Nylon 6. Journal of Reinforced Plastics and Composites, Vol. 23, NO. 7/2004.
2. N Jia and V A. Kagan. (2001). Mechanical Performance of Polyamides with Influence of Moisture and Temperature - Accurate Evaluation and Better Understanding, Plastic Failure: Analysis and Prevention, pp. 95-104, Plastic Design Library (PDL), New York.
3. N Guo, MC Leu. Additive manufacturing; technology, applications and research needs. Front Mechanical Engineering 2013; 8:215-43
4. P Parandoush, D Lin. A review on additive manufacturing of polymer-fiber composites. Composite Structures 182 (2017) 36-53
5. BN Turner, R Strong, SA Gold. A review of melt extrusion additive manufacturing processes: I, Process design and modeling. Rapid Prototyping J 2014;20;192-204
6. M. Vaezi, H. Seitz, S. Yang Int. J. A review on 3D micro-additive manufacturing technologies, Adv. Manuf. Technol. 67 (2013) 1721-1754.
7. X. Wang, M. Jiang, Z. Zhou, J. Gou, D. Hui, 3D printing of polymer matrix composites; a review and prospective, Compos. Part B Eng. 110 (2017) 442–458.
8. H. Prüß, T. Vietor, Design for fiber-reinforced additive manufacturing, J. Mech. Des. 137 (11) (2015) 111409.
9. F. Baumann, J. Scholz, J. Fleischer, Investigation of a new approach for additively manufactured continuous fiber-reinforced polymers, Procedia Cirp 66 (2017) 323–328.
10. A.N. Dickson, J.N. Barry, K.A. McDonnell, D.P. Dowling, Fabrication of continuous carbon, glass and Kevlar fiber reinforced polymer composites using additive manufacturing, Additive. Manuf. 16 (2017) 146–152.
11. W Zhong, F Li, Z Zhang, L Song, Z Li. Short fiber reinforced composites for fused deposition modeling. Mater Sci Eng, A 2001; 301: 125-30

12. O Carneiro, A Silva. R Gomes. Fused deposition modeling with polypropylene. Mater Des 2015; 83: 768-76
13. T. Letcher, M. Waytashek, Material property testing of 3D-printed specimen in PLA on an entry-level 3D printer, in: Proceedings of the ASME 2014 International Mechanical Engineering Congress & Exposition (IMECE2014), Montreal, 2014.
14. T. Letcher, B. Rankouhi, S. Javadpour, Experimental study of mechanical properties of additively manufactured ABS plastic as a function of layer parameters, in: Proceedings of the ASEM 2015 International Mechanical Engineering Congress and Exposition IMECE2015, Houston, 2015.
15. J Ryan, C, Dizon, H Alejandro, Jr Espera, Q Chen, C Rigoberto. Advincula. Review, Mechanical characterization of 3D-printed polymers. Additive Manufacturing 20 (2018) 44-67.
16. R Matsuzaki, M Ueda, M Namiki, Jeong TK, Asahara H, Horiguchi K. Three-dimensional printing of continuous-fiber composites by in-nozzle impregnation. Science Rep 2016;6:23058.
17. M Namiki, M Ueda, A Todoroki, Y Hirano, R Matsuzaki. 3D printing of continuous fiber reinforced plastic. Proceedings of the Society of the Advancement of Material and Process Engineering; 2014.
18. T Yu, J Ren, S Li, H Yuan, Y Li. Effect of fiber surface-treatments on the properties of PLA/ramie composites. Compos A Apply Science Manufacturing 2016; 88: 198-205.
19. A-C Miguel, L-G Ignacio, C-S Nicolette, L L-S Jos é, G-G Teodolito, S C-C Juan, S-B Olga. Evaluation of compressive and flexural properties of continuous fiber fabrication additive manufacturing technology. Additive Manufacturing 22 (2018) 157-164.
20. Talreja R. 2016 Physical modelling of failure in composites. Phil. Trans. R. Soc. A 374: 20150280.
21. S. Ahn, M. Montero, D. Odell, S. Roundy, P.K. Wright, Anisotropic material properties of fused deposition modeling ABS, Rapid Prototype. J. 8 (2002) 248-257

22. Z. Weng, J. Wang, T. Senthil, L. Wu, Mechanical and thermal properties of ABS/montmorillonite nanocomposites for fused deposition modeling 3D printing, Mater. Des. 102 (2016) 276-283.
23. J. Justo, L. T, L. Gar, F. P. Characterization of 3D printed long fiber reinforced composites. Comp Struct 185 (2018) 537-548.
24. Q He, H Wang, K Fu, L Ye. 3D printed continuous CF/PA6 composites: Effect of microscopic voids on mechanical performance. Composites Science and Technology 191 (2020) 108077.
25. M.A Caminero, J.M Chacon, I.G, Interlaminar bonding performance of 3D printed continuous fiber reinforced thermoplastic composites using fused deposition modelling. Polymer Testing 68 (2018) 415-423
26. J. Song and G. W. Ehrenstein, Kunststoffe 80 (1990) 722.
27. G Zhang, C Zhang, P Nardin, W-Y Lia, H Liao, C Coddet. Effects of sliding velocity and applied load on the tribological mechanism of amorphous poly-ether-ether-ketone (PEEK). Tribology International 2008; 41;79-86
28. M. Szpieg, M Wysocki, L E Asp. Mechanical performance and modelling of a fully recycled modified CF/PP composite. Journal of Composite Materials 46(12):1503-1517, June 2012
29. A. G, Airale, M, Carello, A Ferraris, Sisca, L, D Acierno, D Alberto, L Grassia. Moisture effect on mechanical properties of polymeric composite materials. AIP Conference Proceedings, 2016, Vol.1736 (1)
30. ASTM D5229 / D5229M-14. Standard Test Method for Moisture Absorption Properties and Equilibrium Conditioning of Polymer Matrix Composite Materials, ASTM International, West Conshohocken, PA, 2004
31. H Voss, K Friedrich. On the wear behavior of short-fiber-reinforced PEEK composites. Wear 1987; 116:1-18.
32. L. Chang, Z. Zhang. Tribological properties of epoxy nanocomposites Part II. A combinative effect of short carbon fiber with nano-TiO2. Wear 260 2006, 869-878

33. L. Chang, K Friedrich. Enhancement effect of nanoparticles on the sliding wear of short fiber-reinforced polymer composites: A critical discussion of wear mechanisms. Tribol Inter 43, 2010, 2355-2364
34. Jian, L, X, C. The effect of carbon fiber content on the friction and wear properties of carbon fiber reinforced polyimide composites. Wiley InterSci, 25 October 2007.
35. Thorp, J. M. Tribol Inter 1982, 15, 59.
36. M Luo, S Huang, Z Man, J M Cairney, L Chang. Tribological behavior of fused deposition modelling printed short carbon fiber reinforced nylon composites with surface textures under dry and water lubricated conditions. Friction (2022)
37. A Dasari, Z-Z Yu, Y-W Mai. Fundamental aspects and recent progress on wear/scratch damage in polymer nanocomposites. Mater Sci Eng 2009; R 63:31–80.
38. International Organization for standardization, ISO 19252:2008:2008
39. T. Goda, K. V ́aradi, K. Friedrich, H. Giertzsch, Finite element analysis of a polymer composite subjected to a sliding steel asperity Part I Normal fiber orientation, J. Mater. Sci. 37 (8) (2002) 1575–1583.
40. H-X Tang. DC Martin. Journal of Material Science 2003; 38 (4): 803-15.
41. RS Hasdal. RDK Misra. Materials Science and Engineering: A 2005:398 (1-2): 252-261
42. J Han, B Robert, H-J Sue. Understanding of scratch-induced damage mechanisms in polymers. Polymer 50 (2009) 4056-4065
43. A.N. Dickson, J.N. Barry, K.A. McDonnell, D.P. Dowling, Fabrication of continuous carbon, glass and Kevlar fibre reinforced polymer composites using additive manufacturing, Addit. Manuf. 16 (2017) 146–152.
44. Q Cheng, J Han, Y Li. Effect of fiber content and orientation on the scratch behavior of short glass fiber reinforced PBT composites. Tribology International 146 (2020) 106221.

45. S Mzali, S Mezlini, M Zidi. Effect of tribological parameters on scratch behavior of unidirectional E-glass fiber reinforced polyester composite. Tribol Mater Surface Interfac 2013;7:175-82
46. M Bora, O Coban, T Sinmazcelik, V Gunay. Effect of fiber orientation on scratch resistance in unidirectional carbon-fiber-reinforced polymer matrix composites. J Reinforced Plastic Composite 2010;29:1476-90.
47. BKP Wong, SK Sinha, JPY Tan, KY Zeng. Nano-wear mechanism for ultra-high molecular weight polyethylene (uhmwpe) sliding against a model hard asperity. Tribol Lett 2004;17(3):613–22.
48. JL Bucaille, E Felder. Philosophical Magazine A: Physics of Condensed Matter, Structure, Defects and Mechanical Properties 2002;82:2003–12.
49. H Pelletier, C Gauthier, R Schirrer. Proceedings of the Institution of Mechanical Engineers, Part J: Journal of Engineering Tribology 2008;222:221–30.
50. V-K Chandelia. H Sue. M-H Mohammad, FEM Modeling on Scratch Behavior of Multiphase Polymeric Systems. Tribology Letters (2018) 66:62
51. Y L, H T. Micro-scratching of polyethylene terephthalate: Mechanisms of wear debris generation. European Polymer Journal 49 (2013) 1984-1993
52. E Moghbelli, L Sun, H Jiang, W-J Boo, H-J Sue: Scratch behavior of epoxy nanocomposites containing α-zirconium phosphate and core-shell rubber particles. Polym. Eng. Sci. 49, 483–490 (2009)
53. P Kurkcu, L Andena, A Pavan: An experimental investigation of the scratch behavior of polymers—2: influence of hard or soft fillers. Wear 317, 277–290 (2014)
54. J M. Chacon, M A Caminero, Additive manufacturing of PLA structures using fused deposition modelling: effect of interlaminar process parameters on mechanical properties and their optimal selection, Mater. Des 124(2017) 143-157
55. Markforged, Material Data Sheet, (2019)
56. N Jia and V A. Kagan. (2001). Mechanical Performance of Polyamides with Influence of Moisture and Temperature - Accurate Evaluation and Better Understanding, Plastic Failure: Analysis and Prevention, pp. 95-104

57. H Munich. Polyamide, Plastics Handbook, Vol. 4, p. 905, (1998).
58. S Bahadur, D Gong. The role of copper compounds as fillers in the transfer and wear behavior of poly-ether-ether-ketone. Wear 1992; 154: 151-65
59. Standard Test Method for Evaluation of Scratch Resistance of Polymeric Coatings and Plastics Using an Instrumented Scratch Machine. ASTM D7027-13: ASTM International, Pennsylvania.
60. Z Man, B Wan, H Wang, Q Li, L Chang. Experimental and numerical study on scratch performance of additively manufactured continuous carbon fiber reinforced polyamide 6 composites. Composites Science and Technology. 2022, p.109314
61. R Protz, N Kosmann, M Gude, W Hufenbach, K Schulte, B Fiedler. Voids and their effect on the strain rate dependent material properties and fatigue behavior of non-crimp fabric composites materials, Compos. B Eng. 83 (2015) 346–351.
62. A Abdelbary. Wear of polymer on wet condition. Wear of polymers and composites. Woodhead Publishing, Elsevier; 2015. p. 95-112.
63. G T Mark, A S Gozdz, Methods for Composite Filament Fabrication in Three Dimensional Printing, Google Patents, 2015.
64. N W Khun, H Zhang, L H Lim, C Y Yue, X Hu, J Yang. Tribological properties of short carbon fibers reinforced epoxy composites. Friction 2(3): 226-239 (2014)
65. L Chang, Z Zhang, L Ye, K Friedrich. Tribological properties of epoxy nanocomposites: III, Characteristics of transfer films. Wear 262: 699–706 (2007)
66. M F Ashby, J Abulawi, H S Kong. Temperature maps for frictional heating in dry sliding. Tribol Trans 34: 577–587 (1991)
67. W X Chen, F Li, G Han, L Y Wang, J P Tu, Z D Xu. Tribological behavior of carbon nanotube filled PTFE composites. Tribol Lett 15: 275–278 (2003)
68. L Zhang, I Zarudi, K Xiao. Novel behavior of friction and wear of epoxy composites reinforced by carbon nanotubes. Wear 261: 806–811 (2006)
69. J Liu. Material Wear Principle and Wear Resistance; Tsinghua University Press: Beijing. 1993.

70. F Zhao, C Gao, H Wang, T Wang, B Wetzel. B-C Jim, G Zhang, Q Wang. Tribological behaviors of carbon fiber reinforced epoxy composites under PAO lubrication conditions. Tribol Lett (2016) 62:37.

71. Y You, D Li, X Deng, W Li, Y Xie. Tribological properties of solid lubricants filled glass fiber reinforced polyamide 6 composites. Mater Des 46: 809–815 (2013)
72. R Reinicke, F Haupert, K Friedrich. Compos A 1998, 29, 763,
73. M Luo, Q He, H Wang, L Chang. Tribological behavior of surface textured short carbon fiber-reinforced nylon composites fabricated by three-dimensional printing techniques. J Tribol 143(5): 051105 (2021)
74. W Brostow, D Kovacˇevic´, D Vrsaljko, J Whitworth. Tribology of polymers and polymer based composites. J. Mater. Educ. 32(5–6), 273–290 (2010)
75. C.I Chung, W.J Hennessey, M.H Tusim. Frictional behavior of solid polymers on a metal surface at processing conditions. Polymer engineering and science 17(1): 9–20 (1977)
76. T Alomayri, H Assaedi, F.U.A Shaikh, I.M Low. Effect of water absorption on the mechanical properties of cotton fabric-reinforced geopolymer composites. J Asian Ceram Soc 2(3): 223–230 (2014)
77. V Tanrattanakul, N Sungthong, P Raksa. Rubber toughening of nylon 6 with epoxidized natural rubber. Polymer Testing 27 (2008) 794-800
78. Ikramullah, A Afrizal, S Huzni, S Thalib 1, H. P. S. A Khalil, S Rizal. Effect of Mesh Sensitivity and Cohesive Properties on Simulation of Typha Fiber/Epoxy Microbond Test. Computation, 2020, Vol.8 (1), p.2